ARTICLE IN PRESS

Journal of Computational Physics xxx (2011) xxx–xxx

Contents lists available at ScienceDirect

Journal of Computational Physics

journal homepage: www.elsevier.com/locate/jcp

Entropy viscosity method for nonlinear conservation laws ☆

Jean-Luc Guermond [a,*,1], Richard Pasquetti [b], Bojan Popov [a]

[a] Department of Mathematics, Texas A&M University, 3368 TAMU, College Station, TX 77843, USA
[b] Lab. J.A. Dieudonné, UMR CNRS 6621, UNS, 06108 Nice, France

ARTICLE INFO

Article history:
Available online xxxx

Keywords:
Entropy viscosity
Conservation laws
Euler equations
Finite elements
Spectral elements
Fourier method
Godunov schemes
Central schemes

ABSTRACT

A new class of high-order numerical methods for approximating nonlinear conservation laws is described (entropy viscosity method). The novelty is that a nonlinear viscosity based on the local size of an entropy production is added to the numerical discretization at hand. This new approach does not use any flux or slope limiters, applies to equations or systems supplemented with one or more entropy inequalities and does not depend on the mesh type and polynomial approximation. Various benchmark problems are solved with finite elements, spectral elements and Fourier series to illustrate the capability of the proposed method.

© 2010 Elsevier Inc. All rights reserved.

1. Introduction

Solving non-linear hyperbolic systems of conservation laws with high accuracy is a challenging task because high-order methods are known to produce spurious oscillations in shocks. There exists a large class of methods to solve these problems quite efficiently, but to the best of our knowledge all rely at some point on limiters to avoid spurious oscillations. Developing limiters in two and higher space dimension on unstructured meshes with arbitrary polynomial degree is a highly non-trivial task. The theoretical understanding of the stability and convergence of these nonlinear methods is currently limited to uniform grids and scalar equations in one space dimension, see for example [20,22,27,33,34]. A true two-dimensional non-oscillatory reconstruction which could be applied to arbitrary unstructured meshes (without any additional post processing) seems to be available only in the piecewise linear case, see [5,18], and extensions to higher degree polynomial reconstructions do not seem to be evident.

We describe in this paper a new way of generating high-order numerical approximations for nonlinear conservation laws. We avoid the use of limiters and non-oscillatory reconstructions by adding a degenerate nonlinear dissipation to the numerical discretization of the equation or system at hand. The viscosity coefficient is based on the local size of an entropy production. Scalar conservation equations have many entropy pairs and most physical systems have at least one entropy function satisfying an auxiliary entropy inequality. The entropy satisfies a conservation equation only in the regions where the solution is smooth and satisfies an inequality in shocks; this inequality then becomes a selection principle for the physically relevant solution. The amount of violation of the entropy equation is called entropy production. The main idea that we are going to use is that there is a large entropy production in strong shocks (actually it can be proved in simple cases that the

☆ This material is based upon work supported by the National Science Foundation Grant DMS-0713929, DMS-0811041 and by Award No. KUS-C1-016-04, made by King Abdullah University of Science and Technology (KAUST).

* Corresponding author.
E-mail address: guermond@math.tamu.edu (J.-L. Guermond).
[1] On leave from LIMSI, UPRR 3251 CNRS, BP 133, 91403 Orsay Cedex, France.

0021-9991/$ - see front matter © 2010 Elsevier Inc. All rights reserved.
doi:10.1016/j.jcp.2010.11.043

term missing in the entropy inequality to make it an equality is a Dirac measure supported in the shocks). By making the numerical diffusion to be proportional to the entropy production, we add a large numerical dissipation in the shock regions and almost no dissipation in the regions where the solution remains smooth. This simple idea is mesh and approximation independent and can be applied to equations or physical systems that are supplemented with an entropy inequality. This technique has already been shown to be efficient in one space dimension for solving nonlinear conservation laws with Fourier expansions [12].

The paper is organized as follows. The entropy viscosity method for solving scalar conservation laws is described in detail in Section 2. Implementation details for finite elements, spectral elements, and Fourier expansions are also given. Numerical convergence tests on the linear transport equation in one and two-space dimensions are reported in Section 3. The capability of the method to solve nonlinear scalar conservation equations with convex and non-convex fluxes is illustrated is Section 4. An extension of the entropy viscosity method to solve the Euler equations is described in Section 5. All along the paper we emphasize that the method depends only weakly on the space approximation by using different numerical discretizations such as Lagrange finite elements, Fourier expansions, and spectral elements. The numerical results show that this new approach is robust and performs very well in all the considered test cases.

2. Scalar conservation laws

We give in this section a detailed description of the entropy viscosity method for scalar-valued conservations laws.

2.1. The model problem

Let Ω be an open connected domain in $\mathbb{R}^d$. We consider the equation

$$\partial_t u(\boldsymbol{x},t) + \nabla\cdot\boldsymbol{f}(u(\boldsymbol{x},t)) = 0, \quad \boldsymbol{x}\in\Omega, t>0, \tag{2.1}$$

subject to the initial condition $u|_{t=0} = u_0$ and appropriate boundary conditions. In some cases we will solve the Cauchy problem (restricted to a bounded domain) and in other cases we will specify the corresponding boundary conditions. It is well known that the Cauchy or the initial boundary value problem has an unique entropy solution (see [17,3]) which satisfies an additional set of differential inequalities

$$\partial_t E(u) + \nabla\cdot\boldsymbol{F}(u) \leqslant 0 \tag{2.2}$$

for any pairs $E(u)$ and $\boldsymbol{F}(u)$ such that E is convex and $\boldsymbol{F}(u) = \int E'(u)\boldsymbol{f}\,'(u)\mathrm{d}u$. The function E is called entropy and $\boldsymbol{F}$ is the associated entropy flux. The most well known pairs are the Kružkov's pairs generated by $\{E_c(u) := |u-c|, c\in\mathbb{R}\}$. For convex fluxes (i.e., if f is convex) in one space dimension it is known that one entropy pair, for example the one generated by $E(u) = \frac{1}{2}u^2$, is enough to select the unique entropy solution, see for example [6,25].

2.2. The entropy viscosity method

We assume in this section to have at hand a fully centered non-limited, possibly unstable, numerical method for solving nonlinear conservation equations. We are going to construct a nonlinear entropy viscosity to stabilize this method.

Let $u_h(\cdot,t)$ be the numerical approximation of the exact solution u at time t. The entropy viscosity method is constructed along the following lines:

- Given an entropy pair $(E,\boldsymbol{F})$, define the entropy residual:

$$D_h(\boldsymbol{x},t) = \partial_t E(u_h(\boldsymbol{x},t)) + \nabla\cdot\boldsymbol{F}(u_h(\boldsymbol{x},t)), \quad \boldsymbol{x}\in\Omega,\ t>0. \tag{2.3}$$

- Use this residual to define a viscosity, say ν_E:

$$\nu_E(\boldsymbol{x},t) := c_E h^2(\boldsymbol{x}) R(D_h(\boldsymbol{x},t))/\|E(u_h) - \overline{E}(u_h)\|_{\infty,\Omega}, \tag{2.4}$$

  where $h(\boldsymbol{x})$ is the local mesh size at $\boldsymbol{x}\in\Omega$, $\overline{E}$ is the space-averaged value of the entropy, c_E is a tunable constant and R is a positive functional that remains to be specified. Since D_h is expected to oscillate, and this is especially true if a shock develops since D_h approximates a Dirac measure in this case, the simplest functional that one can use to avoid negative values is $R(D_h) = |D_h|$. Introducing the scaling coefficient $h^2(\boldsymbol{x})$ together with the normalizing term $\|E(u_h) - \overline{E}(u_h)\|_{\infty,\Omega}$ gives to ν_E the dimension of a viscosity.
- Introduce an upper bound to the entropy viscosity:

$$\nu_{\max}(\boldsymbol{x},t) := c_{\max} h_{\max}(\boldsymbol{x}) \max_{\boldsymbol{y}\in V_{\boldsymbol{x}}} |\boldsymbol{f}\,'(u(\boldsymbol{y},t))|. \tag{2.5}$$

  Here $V_{\boldsymbol{x}}$ is a yet to be defined neighborhood of $\boldsymbol{x}$, $\boldsymbol{f}'(u(\boldsymbol{y},t))$ is the local wave speed (recall $\nabla\cdot\boldsymbol{f}(u) = \boldsymbol{f}'(u)\cdot\nabla u$). When using finite differences on a one-dimensional uniform grid, setting $c_{\max} = \frac{1}{2}$ corresponds to replacing the centered differences by first-order upwind differences which are known to be monotone. Note that the quantity $h(\boldsymbol{x})$ used in (2.4) may differ from $h_{\max}(\boldsymbol{x})$ which is used in (2.5), which is indeed the case when we use spectral finite elements, see Section 2.4.

Please cite this article in press as: J.-L. Guermond et al., Entropy viscosity method for nonlinear conservation laws, J. Comput. Phys. (2011), doi:10.1016/j.jcp.2010.11.043

- Define the entropy viscosity:

$$v_h := S(\min(v_{\max}, v_E)), \tag{2.6}$$

where S is a yet to be defined smoothing operator that depends on the space approximation.
- Augment the discrete form of the conservation law (2.1) with the dissipation term $-\nabla\cdot(v_h\nabla u_h)$ and make the viscosity explicit.

In order to further describe the entropy viscosity method, we have to specify the numerical discretization. Implementation details, especially concerning suitable definitions of the functional R and the operator S, depend on the numerical approximation. Our implementations of the method for finite elements, spectral elements, and Fourier expansions are described hereafter.

The above method is simple to implement, but simplicity has a price and the price paid here is the introduction of two tunable constants c_E and $c_{\max}$. In practice these two constants are tuned by testing the method on a coarse grid. For any given problem, the tuning is done quickly once and for all on a coarse mesh. Details on the tuning procedure are reported in Section 2.7.

Remark 2.1. The idea of using the entropy to design numerical methods for nonlinear conservation equations is not new. For instance it is shown in [2,28] that the entropy production can be used an a posteriori error indicator and therefore useful for adaptive strategies. The main originality of the work presented here is that we directly use the entropy production to construct an artificial viscosity.

Remark 2.2. Using a residual to construct a viscosity is not a new idea, we refer to [13,15,31] where it is the residual of the conservation equation which is used. Although the residual of the conservation equation (2.1) is a good error indicator, it is far less robust than the entropy residual (2.2) since consistency requires that the residual converges to zero in the distribution sense as the mesh-size goes to zero. In other words, the equation residual must eventually vanish almost everywhere, whereas the entropy residual converges to a Dirac measure supported in the shocks, and it is in this sense that we mean that the entropy residual is more robust than the residual of the conservation equation.

2.3. Finite element approximation

We call a mesh $\mathcal{T}_h$ a subdivision of Ω into disjoint elements K such that $\overline{\Omega} = \cup_{K\in\mathcal{T}_h}\overline{K}$; $\overline{\Omega}$ and $\overline{K}$ are the closure of Ω and K, respectively. The mesh is assumed to be affine to avoid unnecessary technicalities, i.e., Ω is assumed to be a polygon in two space dimensions or a polyhedron in three space dimensions. We suppose that we have at hand a family of meshes $\{\mathcal{T}_h\}_{h>0}$ and that this family is shape-regular and each mesh is conforming.

For each mesh $\mathcal{T}_h$ we define a continuous approximation space as follows:

$$X_h = \{v_h \in \mathcal{C}^0(\overline{\Omega});\ \forall K \in \mathcal{T}_h,\ v_h|_K \circ \boldsymbol{g}_K \in P_k\}, \tag{2.7}$$

where $\boldsymbol{g}_K$ maps the reference element $\widehat{K}$ to the element K and P_k is a vector space composed of polynomials defined over $\widehat{K}$. We assume that $\mathbb{P}_k \subset P_k$, where $\mathbb{P}_k$ denotes the set of polynomials of total degree at most $k \geqslant 1$.

For each $K \in \mathcal{T}_h$ we define the following quantities:

$$h_K \text{ is the smallest edge of } K, \tag{2.8}$$

$$R(D_h(\boldsymbol{x},t)) := \|D_h\|_{\infty,K}, \quad \forall \boldsymbol{x} \in K, \tag{2.9}$$

$$v_E|_K := c_E h_K^2 \frac{\|D_h\|_{\infty,K}}{\|E(u_h) - \overline{E}(u_h)\|_{\infty,\Omega}}. \tag{2.10}$$

The viscosity v_E is thus piecewise constant. In the finite element framework it is natural to set $V_{\boldsymbol{x}} := K \ni \boldsymbol{x}$ and $h_{\max}(\boldsymbol{x}) = h_K$, so that

$$v_{\max}|_K := c_{\max} h_K \|\boldsymbol{f}'(u)\|_{\infty,K}. \tag{2.11}$$

Whenever an infinity norm over K is invoked, the norm is approximated by evaluating the maximum of the quantity in question over the quadrature Gauss points in K. The viscosity v_h is obtained by setting $S = I$ (i.e., no smoothing is applied) so that

$$v_h = \min(v_{\max}, v_E). \tag{2.12}$$

Finally the solution method is based on the Galerkin formulation of the stabilized equation, that is

$$\int_\Omega (\partial_t u_h + \nabla\cdot\boldsymbol{f}(u_h))v_h \mathrm{d}\boldsymbol{x} + \sum_K v_h \int_K \nabla u_h \cdot \nabla v_h \mathrm{d}\boldsymbol{x} = 0, \quad \forall v_h \in X_h. \tag{2.13}$$

Details on the time stepping are given in Section 2.6.

Please cite this article in press as: J.-L. Guermond et al., Entropy viscosity method for nonlinear conservation laws, J. Comput. Phys. (2011), doi:10.1016/j.jcp.2010.11.043

2.4. Spectral element approximation

When using the spectral element method we assume that the mesh $\mathcal{T}_h$ is composed of segments, quadrangles or hexahedrons in one, two and three space dimensions, respectively. Each mesh cell K is the image by a map $\boldsymbol{g}_K$ of the reference element $\widehat{K} = (-1,1)^d$, where d is the space dimension. The approximation u_h is continuous in space and $u_h|_K \circ \boldsymbol{g}_K \in \mathbb{Q}_k$, where $\mathbb{Q}_k$ is the space of the polynomials of degree at most $k \geqslant 2$ in each variable. The spectral element shape functions are the Lagrange polynomials based on the $k+1$ Gauss–Lobatto–Legendre (GLL) points in 1D and are tensor products thereof in higher space dimension. The quadrature are also based on the GLL points so that the interpolation and quadrature points coincide. As a result, the mass matrix is diagonal. Details can be found in [7].

Since the distance between GLL points may have large variations over one element it is suitable to use a local value of the grid size. This may be done in several ways with actually weak influence on the results. In the simplest approach we define the quantity $h(\boldsymbol{x})$ to be the distance of the considered interpolation/quadrature point to the closest one. To be more specific, assume that we are in two-space dimension and denote $\{\boldsymbol{x}_{i,j}\}_{i,j=0,\ldots,k} =: \mathrm{GLL}_K$, the images by $\boldsymbol{g}_K$ of the GLL points, then we set:

$$h(\boldsymbol{x}_{i,j}) := \min_{\boldsymbol{x}_{ij} \neq \boldsymbol{x}_{i'j'} \in \mathrm{GLL}_K} |\boldsymbol{x}_{i,j} - \boldsymbol{x}_{i'j'}|, \quad \forall \boldsymbol{x}_{i,j} \in \mathrm{GLL}_K, \tag{2.14}$$

$$R(D_h(\boldsymbol{x}_{i,j},t)) := |D_h(\boldsymbol{x}_{i,j},t)|, \quad \forall \boldsymbol{x}_{i,j} \in \mathrm{GLL}_K,\ \forall t > 0, \tag{2.15}$$

$$v_E(\boldsymbol{x}_{i,j},t) := c_E h^2(\boldsymbol{x}_{i,j}) \frac{|D_h(\boldsymbol{x}_{i,j},t)|}{\|E(u_h) - \overline{E}(u_h)\|_{\infty,\Omega}} \quad \forall \boldsymbol{x}_{i,j} \in \mathrm{GLL}_K,\ \forall t > 0. \tag{2.16}$$

The maximum viscosity is defined by setting $V_{\boldsymbol{x}} = K \ni \boldsymbol{x}$ and $h_{\max}(\boldsymbol{x}) = h_K$. The maximum viscosity is piecewise constant over each element and defined to be

$$v_{\max}|_K = c_{\max} h_K \max_{\boldsymbol{x}_{i,j} \in \mathrm{GLL}_K} |\boldsymbol{f}'(u_h(\boldsymbol{x}_{i,j},t))| \tag{2.17}$$

Numerical experiments show that using $S = I$ leaves some small oscillations when the polynomial degree k is large. These residual oscillations can be removed by slightly smoothing the viscosity. Smoothing of the viscosity may be theoretically justified [1] and is introduced to remedy the fact that the computation of the viscosity is explicit, i.e., the computation of the entropy viscosity lags in time. Smoothing is done over each element on the GLL mesh. For instance, again in two-space dimensions the operator S is defined as follows at the interior points $\{\boldsymbol{x}_{i,j}\}_{i,j=1,\ldots,k-1}$:

$$S(\varphi)(\boldsymbol{x}_{i,j}) = \frac{1}{8}(\varphi(\boldsymbol{x}_{i-1,j}) + \varphi(\boldsymbol{x}_{i,j+1}) + \varphi(\boldsymbol{x}_{i+1,j}) + \varphi(\boldsymbol{x}_{i,j-1}) + 4\varphi(\boldsymbol{x}_{ij})). \tag{2.18}$$

A similar formula is used at the boundary points assuming symmetry; for instance, whenever the value $\varphi(\boldsymbol{x}_{i\pm1,j})$ (resp. $\varphi(\boldsymbol{x}_{i,j\pm j})$) does not exist, $i,j \in \{0,k\}$, it is then replaced by $\varphi(\boldsymbol{x}_{i\mp1,j})$ (resp. $\varphi(\boldsymbol{x}_{i,j\mp1})$). Note that when applied to functions showing point to point oscillations with two different values, such formula provide the mean value constant function.

2.5. Fourier approximation

We now extend the work done in [12] and show how the method can be used with Fourier expansions in two and higher space dimensions.

We assume that the computational domain Ω is the cube $(0,1)^d$ or an affine image thereof and the solution is Ω-periodic. Let $N \geqslant 1$ be a positive integer and set $h = (2N)^{-1}$. A Fourier approximation

$$u_h = \sum_{\|\boldsymbol{k}\|_\infty \leqslant N} \hat{u}_{\boldsymbol{k}}(t) \exp(2\mathrm{i}\pi \boldsymbol{k}\cdot\boldsymbol{x}), \quad \hat{u}_{-\boldsymbol{k}} = \bar{\hat{u}}_{\boldsymbol{k}}, \quad \mathrm{i}^2 = -1, \tag{2.19}$$

to (2.1) is defined by solving

$$\partial_t u_h + \nabla\cdot(P_N \boldsymbol{f}(u_h)) = \nabla\cdot(P_N(v_h(u_h)\nabla u_h)), \quad u_h(\boldsymbol{x},0) = P_N u_0, \tag{2.20}$$

where P_N is the L^2-projection onto the trigonometric polynomials of degree at most N. The L^2-projection of nonlinear terms is evaluated by using a pseudo-spectral method and the $\frac{3}{2}$ padding rule for de-aliasing.

Let $\{\boldsymbol{x}_{\boldsymbol{l}}\}$ be the set of collocation points in the physical space: $\boldsymbol{x}_{\boldsymbol{l}} = h\boldsymbol{l}, \boldsymbol{l} := (\ell_1,\ldots,\ell_d) \in \mathbb{N}^d, 0 \leqslant \ell_i \leqslant 2N-1$. Then we set

$$h(\boldsymbol{x}_{\boldsymbol{l}}) := h, \quad \forall \boldsymbol{x}_{\boldsymbol{l}}, \tag{2.21}$$

$$R(D_h(\boldsymbol{x}_{\boldsymbol{l}},t)) := |D_h(\boldsymbol{x}_{\boldsymbol{l}},t)|, \quad \forall \boldsymbol{x}_{\boldsymbol{l}},\ \forall t > 0, \tag{2.22}$$

$$v_E(\boldsymbol{x}_{\boldsymbol{l}},t) := c_E h^2(\boldsymbol{x}_{\boldsymbol{l}}) |D_h(\boldsymbol{x}_{\boldsymbol{l}},t)| / \|E(u_h) - \overline{E}(u_h)\|_{\infty,\Omega} \quad \forall \boldsymbol{x}_{\boldsymbol{l}},\ \forall t > 0. \tag{2.23}$$

To evaluate the maximum viscosity we set $h_{\max}(\boldsymbol{x}) = h$ and denote by $V_{\boldsymbol{x}}$ the set of $(2s+1)^d$ collocation points contained in the cube centered at $\boldsymbol{x}$ and of side $2sh$, (in practice we take $s = 3$) and we set

$$v_{\max}(\boldsymbol{x},t) = c_{\max} h \max_{\boldsymbol{x}_{\boldsymbol{l}} \in V_{\boldsymbol{x}}} |\boldsymbol{f}'(u_h(\boldsymbol{x}_{\boldsymbol{l}},t))|. \tag{2.24}$$

Finally we set $v_h(\boldsymbol{x}) = S(\min(v_{\max}, v_E))$ where S is the d-dimensional variant of smoothing operator defined in (2.18).

Please cite this article in press as: J.-L. Guermond et al., Entropy viscosity method for nonlinear conservation laws, J. Comput. Phys. (2011), doi:10.1016/j.jcp.2010.11.043

2.6. Details on the time-stepping

Even though other time stepping methods could be considered (like BDF2 or higher), we assume from now on that the advancement in time is done by means of an explicit Runge–Kutta method identified by the following Butcher tableau:

$$\begin{array}{c|ccccc} 0 & & & & & \\ c_2 & a_{21} & & & & \\ c_3 & a_{31} & a_{32} & & & \\ \vdots & \vdots & & \ddots & & \\ c_s & a_{s1} & a_{s2} & \cdots & a_{s,s-1} & \\ \hline & b_1 & b_2 & \cdots & b_{s-1} & b_s \end{array} \tag{2.25}$$

Remark 2.3. All the tests reported in this paper have been done using either the standard explicit RK4 method or the SSP RK3 method, see [10]; the corresponding Butcher tableaux are shown in Table 2.1.

Let Δt be the time step. Let u_h^n, u_h^{n-1}, etc. be the approximations of the solution at times t_n, t_{n-1}, etc. We define the values of the entropy function: $E_h^n := E(u_h^n), E_h^{n-1} := E(u_h^{n-1})$, etc. The next task consists of evaluating the entropy residual. There are many ways to do that. If the time step is constant, one possible option consists of setting:

$$D_h = \frac{1}{2\Delta t}\left(3E_h^n - 4E_h^{n-1} + E_h^{n-2}\right) + \boldsymbol{f}\,'(u_h^n)\cdot\nabla E(u_h^n). \tag{2.26}$$

This is an explicit evaluation of the entropy residual at time t_n where the time derivative $\partial_t E(u_h(x,t_n)$ is replaced by the second-order backward finite difference (a similar formula can be deduced if the time step is not constant). Since this is a second-order evaluation of the entropy residual at t_n, the entropy viscosity is $\mathcal{O}(h^2\Delta t^2)$ if the solution is smooth, i.e., the induced viscosity is fourth-order if P_1 approximation is used in space. Whether D_h is only a first-order approximation of $D(u_h(\cdot,t))$ for $t\in[t_n,t_{n+1}]$ does not matter since the error thus made in smooth regions is $\mathcal{O}(h^2\Delta t^3)$. In the vicinity of shocks and sharp fronts, the error made in $\mathcal{O}(h\Delta t)$ which is still fine since in these regions the $\mathcal{O}(h)$ viscosity make the method first-order accurate anyway. They are many other consistent ways of constructing D_h; in particular D_h can also be evaluated on the fly by embedding the computation between the Runge–Kutta substeps.

Then, the next step consists of evaluating the viscosities ν_E and $\nu_{\max}$, which depend on the tunable coefficients c_E and $c_{\max}$. These coefficients depend of the time-marching technique and of the space approximation method, but are independent of time step Δt and the mesh-size, see Section 2.7.

Once the entropy viscosity field ν_h is available, we define the operator $F_h : L^1(\Omega)\times\mathbb{R}\to X_h$ so that $F_h(v,t)$ solves the following problem

$$\int_\Omega F_h(v,t)w_h\,\mathrm{d}\boldsymbol{x} = -\sum_{K\in\mathcal{T}_h}\int_K (w_h\nabla\cdot\boldsymbol{f}(v(\boldsymbol{x},t)) + \nu_h\nabla v\cdot\nabla w_h)\,\mathrm{d}\boldsymbol{x},\quad w_h\in X_h. \tag{2.27}$$

Computing F_h amounts to solving a mass matrix problem. This is trivial when the mass matrix is diagonal, which is the case for the Fourier and the spectral element method; in any case it is always an easy task. The time consuming part of the algorithm consists of computing the right-hand side of (2.27).

We then recursively compute

$$\begin{cases} k_1 = F_h\left(u_h^n, t_n\right), \\ k_2 = F_h\left(u_h^n + a_{21}\Delta t k_1, t_n + c_2\Delta t\right), \\ \vdots \\ k_s = F_h\left(u_h^n + a_{s1}\Delta t k_1 + a_{s2}\Delta t k_2 + \cdots + a_{s,s-1}\Delta t k_{s-1}, t_n + c_s\Delta t\right) \end{cases} \tag{2.28}$$

and the solution at $t_{n+1} := t_n + \Delta t$ is $u_h^{n+1} = u_h^n + \Delta t\sum_{i=1}^s b_i k_i$.

Table 2.1
Butcher tableau for the explicit SSP RK3 (left) and RK4 (right) methods that are used.

$$\begin{array}{c|ccc} 0 & & & \\ 1 & 1 & & \\ \frac{1}{2} & \frac{1}{4} & \frac{1}{4} & \\ \hline & \frac{1}{6} & \frac{1}{6} & \frac{2}{3} \end{array} \qquad \begin{array}{c|cccc} 0 & & & & \\ \frac{1}{2} & \frac{1}{2} & & & \\ \frac{1}{2} & 0 & \frac{1}{2} & & \\ 1 & 0 & 0 & 1 & \\ \hline & \frac{1}{6} & \frac{1}{3} & \frac{1}{3} & \frac{1}{6} \end{array}$$

2.7. Tuning of c_E and c_{max}

The strategy which is systematically adopted to set the coefficients c_E and $c_{\max}$ is the following. First, we set $c_E = \infty$ so that only the first-order viscosity is active: $\nu_h = \nu_{\max}$. Then the coefficient $c_{\max}$ is tuned to be as small as possible so that the computed solution is smooth and the time marching is stable. A typical range is $c_{\max} \in [0.15, \frac{1}{2}]$. For instance, assuming that the space dimension is one and $\mathbf{f}(u) = \beta u \boldsymbol{e}_x$ (i.e., linear transport), if the transport term is approximated with uniform centered second-order finite differences, setting $c_{\max} = \frac{1}{2}$ is exactly equivalent to first-order up-winding. More precisely, assume that $\beta \geqslant 0$ so that $\nabla \cdot \boldsymbol{f}(u) = \beta \partial_x u$ and approximate $\partial_x u$ using the upwind finite difference, then

$$\nabla \cdot \boldsymbol{f}(u)(x_i) \approx \beta \frac{u_i - u_{i-1}}{h} = \beta \frac{u_{i+1} - u_{i-1}}{2h} - \frac{1}{2}|\beta| h \frac{u_{i+1} - 2u_i + u_{i-1}}{h^2}.$$

This equality indeed proves that the centered second-order finite difference plus a diffusion of order $\frac{1}{2}|\beta|h$ is equivalent to up-winding. Our experience is that $c_{\max} = \frac{1}{2}$ is always a good first guess. Once $c_{\max}$ is chosen, set $c_E = 1$ and then reduce the value of c_E as much as possible until the solution is on the verge of loosing smoothness or stability. A typical range is $c_E \in [0.1, 1]$. For any given problem, the tuning is done quickly once and for all on a very coarse mesh.

3. Linear conservation laws

In this section we evaluate the convergence properties of the entropy viscosity method on the scalar-valued linear transport equation:

$$\partial_t u + \boldsymbol{\beta} \cdot \nabla u = 0, \quad u|_{t=0} = u_0, \quad u|_{\partial\Omega^-} = 0, \tag{3.1}$$

where $\boldsymbol{\beta}$ is a smooth vector field, $\boldsymbol{n}$ is the unit outward normal vector at the boundary, $\partial\Omega^- = \{\boldsymbol{x} \in \partial\Omega | \boldsymbol{n}(\boldsymbol{x}) \cdot \boldsymbol{\beta}(\boldsymbol{x}) < 0\}$ is the inflow boundary. We assume that u_0 and the vector field $\boldsymbol{\beta}$ are smooth enough to guaranty well-posedness of the problem in a reasonable setting.

One can define an entropy for the linear transport equation in many ways, for instance one can set $E_h(u_h) := u_h$ or $E_h(u_h) := |u_h|^p$, $p \geqslant 1$. Henceforth we choose $E_h(u_h) = \frac{1}{2}u_h^2$.

3.1. Linear transport in 1D

We test the convergence properties of the method with respect to the mesh size in one space dimension by using the spectral element method in space. The time marching is done with the explicit RK4 method so that the error induced by the time discretization is significantly smaller than the error with respect to space discretization.

3.1.1. Model problem and discretization

The domain is $\Omega = (0,1)$ and the model problem is

$$\partial_t u + \partial_x u = 0, \quad u \text{ periodic}, \quad u(x,0) = u_0(x), \quad x \in \Omega. \tag{3.2}$$

The transport velocity is equal to unity ($\beta = 1$) and the boundary conditions are periodic. The exact solution is $u(x,t) = u_0(x-t)$.

We use polynomials of degree $k = 1, \ldots, 8$. To avoid super-convergence phenomena the size of each cell is chosen randomly under the constraint that the maximum size ratio over the mesh is 2.

3.1.2. Convergence tests

We start with the initial data $u_0(x) = \sin(4\pi x)$, which implies that the exact solution is infinitely smooth in this case. For each polynomial degree $k = 1, \ldots, 8$, we perform four computations up to $t = 1$ on meshes composed of $80/k$, $160/k$, $320/k$, and $640/k$ cells. For all the tests reported hereafter the viscosity coefficients are $c_{\max}(k) = 0.1/k$ and $c_E = 1$.

Let $\mathcal{T}_h$ and $\mathcal{T}_{h/2}$ be two consecutive meshes and let e_h, $e_{h/2}$ be some errors measured in some norm on these meshes; we call convergence rate with respect to the mesh size the ratio $\log(e_h/e_{h/2})/\log(2)$. For the smooth initial data considered here, we observe that both the Galerkin and the entropy viscosity solutions have optimal convergence order $\mathcal{O}(h^r), r = \min(k+1, 4)$ due to the use of a RK4 scheme, independently of the L^p-norm.

We now consider a non-smooth initial data: $u_0(x) = 1$ if $|x - \frac{1}{2}| \leqslant \frac{1}{4}$ and $u_0(x) = 0$ otherwise. The solution is only in BV (Ω) and in $H^{\frac{1}{2}-\epsilon}(\Omega)$, $\epsilon > 0$. Therefore, the theoretically best approximation orders with respect to the mesh size in L^1 and in L^2 are 1 and $\frac{1}{2}$, respectively. The observed convergence rates for this problem are reported in Table 3.1. The symbol Gal. labels the results for the Galerkin solution (no viscosity, $c_{\max} = c_E = 0$). The symbol Vis. labels the results for the first-order viscosity solution ($c_E = \infty$). The symbol Ent. labels the results obtained for the entropy viscosity method.

We observe that the entropy viscosity solution has a higher convergence rate than both the Galerkin and the first-order viscosity solution in the L^1-norm. The Galerkin and entropy solutions show similar rates in the L^2-norm, which of course are higher than that of the first-order viscosity. The convergence rates of the entropy viscosity solution converge to the theoretical limits 1 and $\frac{1}{2}$ in the L^1- and L^2-norm as k grows, respectively.

Please cite this article in press as: J.-L. Guermond et al., Entropy viscosity method for nonlinear conservation laws, J. Comput. Phys. (2011), doi:10.1016/j.jcp.2010.11.043

Table 3.1
1D convergence tests on a non-smooth solution.

Norm	Method	$\mathbb{P}_1$	$\mathbb{P}_2$	$\mathbb{P}_3$	$\mathbb{P}_4$	$\mathbb{P}_5$	$\mathbb{P}_6$	$\mathbb{P}_7$	$\mathbb{P}_8$
L^1	Gal.	0.42	0.59	0.62	0.74	0.85	0.80	0.89	0.94
	Vis.	0.51	0.54	0.54	0.55	0.56	0.58	0.58	0.60
	Ent.	0.70	0.77	0.83	0.88	0.91	0.84	0.91	0.95
L^2	Gal.	0.31	0.40	0.39	0.47	0.49	0.49	0.46	0.54
	Vis.	0.26	0.27	0.27	0.28	0.28	0.29	0.28	0.31
	Ent.	0.37	0.39	0.41	0.45	0.46	0.45	0.46	0.52

3.1.3. Long time integration

We now test the behavior of the method when the final time is large. The domain is still $\Omega = (0,1)$ and the transport problem is the same as above but the initial data is now

$$u_0(x) = \begin{cases} e^{-300(2x-0.3)^2} & \text{if } |2x-0.3| \leqslant 0.25, \\ 1 & \text{if } |2x-0.9| \leqslant 0.2, \\ \left(1-\left(\frac{2x-1.6}{0.2}\right)^2\right)^{\frac{1}{2}} & \text{if } |2x-1.6| \leqslant 0.2, \\ 0 & \text{otherwise.} \end{cases} \tag{3.3}$$

This test case is documented in [30]. We compute the solution at $t = 100$, i.e., the domain has been traversed 100 times, and we use polynomial degrees $k = 2,\ldots,8$. The mesh is composed of $200/k$ cells so that the total number of degrees of freedom is 200. The numerical results are shown if Fig. 3.1.

The Galerkin solution is shown in the left panel. The solution in the center panel is computed by using the constant first-order viscosity $\nu_{\max} = c_{\max} h_K$. The entropy solution is shown in the right panel. This test shows that the Galerkin solutions is very oscillatory and unusable for any practical purpose. The first-order viscous solution is almost constant. The viscosity has dampened the large scale features of the solution and the approximate solution is close to the space average of u_0. The entropy solution is qualitatively superior to both the Galerkin and the first-order viscous solution. We observe that the higher the polynomial degree the more accurate is the approximation.

3.1.4. Comparison with linear stabilization

Many linear stabilization techniques are known to be very effective for solving the linear transport equation, (see e.g., subgrid viscosity [11], edge stabilization [4,8], Discontinuous Galerkin). All these methods are known to give near optimal convergence order $\mathcal{O}\left(h^{k+\frac{1}{2}}\right)$.

We now illustrate how the entropy viscosity method compares with one of these method on the above one-dimensional transport problem with initial data (3.3). The linear stabilization method which is used is the edge stabilization (the coefficient multiplying the edge stabilization term is 0.05); the choice of the method is not important since they all have the same convergence properties. The mesh distribution is random so that the size ratio of two consecutive mesh cells can be at most 3. Randomness is introduced to limit super-convergence phenomena.

We show the results at time $t = 1$ in the left panel of Fig. 3.2 and the results at time 100 in the right panel. The dot-dashed line is the exact solution, the solid line is the entropy viscosity solution, and the dashed line is the edge stabilized solution. At $t = 1$ the edge stabilized solution under-shoots and over-shoots; this is the well-known Gibbs phenomenon. The amplitude of these under-shoots and over-shoots is constant and bounded away from zero irrespective of the mesh size. The entropy viscosity solution does not suffer from this problem. At $t = 100$ the edge stabilized solution suffers from over dissipation when compared to the entropy viscosity solution.

The provisional conclusion one is lead to draw from this simple test is that linear stabilized methods may be slightly superior to the entropy viscosity method in terms of accuracy since they can be proved to be $\mathcal{O}\left(h^{k+\frac{1}{2}}\right)$ accurate, but these methods

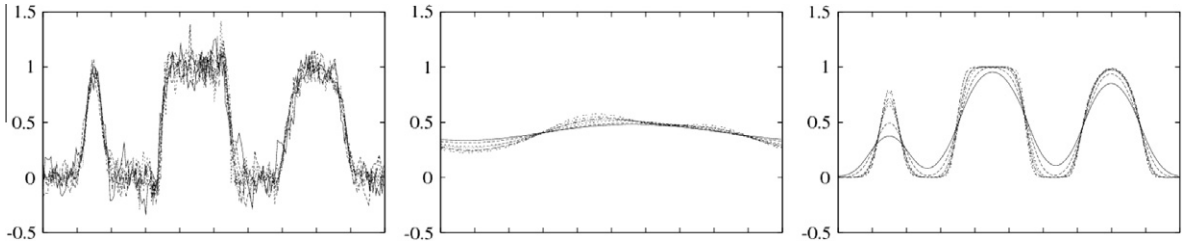

Fig. 3.1. Long time integration, $t = 100$, for polynomial degrees $k = 2,\ldots 8$, #d.o.f. = 200. Galerkin (left); Constant viscosity (center); Entropy viscosity (right).

Please cite this article in press as: J.-L. Guermond et al., Entropy viscosity method for nonlinear conservation laws, J. Comput. Phys. (2011), doi:10.1016/j.jcp.2010.11.043

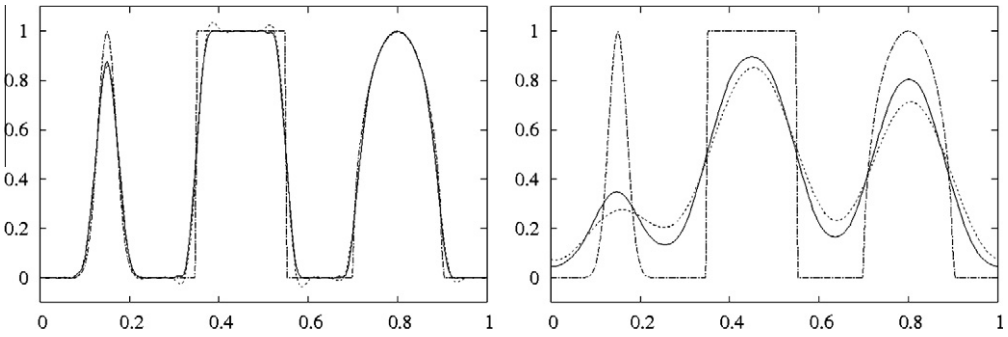

Fig. 3.2. Dot-dashed line is the exact solution, solid line is the entropy viscosity solution, dashed line is the edge stabilized solution. Solutions at $t = 1$ (Left), solutions at $t = 100$ (Right).

are clearly inferior to the entropy viscosity method when it comes to solving non-smooth problems, which is the main topic of this paper. Actually we have observed that when applied to some nonlinear conservations equations with non-convex fluxes linear stabilization methods give solutions that converge to weak solutions that violate the entropy condition whereas the entropy viscosity method converges to the correct solution, (see for instance the non-convex flux proposed in [(3)][16] and [Section 3.1][19]).

Remark 3.1. The computation reported in Fig. 3.2 have been done with $\mathbb{P}_1$ finite elements and RK4. The algorithm is stable up to $CFL = 1.5$. The entropy viscosity has been computed as follows:

$$D_h|_{[x_i,x_{i+1}]} = \max\left(\left|\frac{\Delta E(x_i))}{2\Delta t} + \frac{E(u_h^n(x_{i+1})) - E(u_h^n(x_i))}{h_{i+\frac{1}{2}}}\right|, \left|\frac{\Delta E(x_{i+1}))}{2\Delta t} + \frac{E(u_h^n(x_{i+1})) - E(u_h^n(x_i))}{h_{i+\frac{1}{2}}}\right|\right), \tag{3.4}$$

$$\Delta E(x) := \frac{3E(u_h^n(x)) - 4E(u_h^{n-1}(x)) + E(u_h^{n-2}(x))}{2\Delta t}, \quad h_{i+\frac{1}{2}} := |x_{i+1} - x_i|, \tag{3.5}$$

$$\mu_h|_{[x_i,x_{i+1}]} = \max\left(c_{\max} h_{i+\frac{1}{2}}, c_E h_{i+\frac{1}{2}}^2 D_h|_{[x_i,x_{i+1}]} / \max_j |E(x_j) - \overline{E}|\right), \quad c_{\max} = \frac{1}{2}, c_E = \frac{1}{4}, \tag{3.6}$$

$$\overline{E} = \sum_i \frac{h_{i+\frac{1}{2}}}{2}\left(E(u_h^n(x_i)) + E(u_h^n(x_i))\right) / \sum_i h_{i+\frac{1}{2}}. \tag{3.7}$$

3.2. Linear transport in 2D

We now illustrate the method in two space dimensions. The domain is $\Omega = \{(x,y) \in \mathbb{R}^2, \sqrt{x^2+y^2} \leqslant 1\} := B(0,1)$, and the model problem is a solid rotation about the origin with angular speed 2π

$$\partial_t u + \boldsymbol{\beta} \cdot \nabla u = 0, \quad u|_{t=0} = u_0, \tag{3.8}$$

where $\boldsymbol{\beta} = 2\pi(-y,x)$. The exact solution is $u(x,y) = u_0(r\cos(\theta - 2\pi t), r\sin(\theta - 2\pi t))$, where $r = \sqrt{x^2+y^2}$ and $\theta = \arctan(y/x)$ are the cylindrical coordinates.

3.2.1. Finite element approximation

The method is implemented using the explicit RK4 time stepping. Space approximation is done using $\mathcal{C}^0$ triangular finite elements $\mathbb{P}_1$ and $\mathbb{P}_2$. The meshes are unstructured and are created using a frontal Delaunay mesh generator [29]. The mass matrix problems are solved using GMRES preconditioned with thresholded ILU (k). For all the test reported in this section the control parameters of the entropy viscosity are $c_{\max} = 0.1/k$ and $c_E = 0.5$.

The accuracy with respect to space is evaluated by considering the smooth solution to (3.8) generated by the initial condition $u_0(x,y) = \frac{1}{2}\left(1 - \tanh\left(\frac{(x-r_0)^2+y^2}{a^2} - 1\right)\right)$, with parameters $a = 0.3$, $r_0 = 0.4$.

The test are done up to $t = 1$ on seven meshes with typical mesh size $h = 0.2, 0.1, 0.05, 0.025; 0.0125, 0.01, 0.00625$. The errors measured in the L^1- and L^2-norms are reported in Table 3.2 for the $\mathbb{P}_1$ approximation and in Table 3.3 for $\mathbb{P}_2$ approximation. The notation is the same as in Section 3.1.2. We observe that the $\mathbb{P}_1$ approximation is second-order both in the L^1- and L^2-norms. We also observe that the $\mathbb{P}_2$ approximation is only second-order both in the L^1- and L^2-norms, i.e., the $\mathbb{P}_2$ approximation is slightly suboptimal. Actually, since the entropy–viscosity perturbation vanishes when the solution is smooth, the entropy viscosity method reduces to the Galerkin method for smooth solutions; as a result, the entropy viscosity

Please cite this article in press as: J.-L. Guermond et al., Entropy viscosity method for nonlinear conservation laws, J. Comput. Phys. (2011), doi:10.1016/j.jcp.2010.11.043

Table 3.2
Rotating transport with smooth solution, $\mathbb{P}_1$ approximation.

h	$\mathbb{P}_1$ Ent.				$\mathbb{P}_1$ Gal.			
	L^1	Rate	L^2	Rate	L^1	Rate	L^2	Rate
2.00E−1	3.61E−1	–	2.59E−1	–	2.79E−1	–	1.71E−1	–
1.00E−1	1.32E−1	1.45	9.79E−2	1.40	1.15E−1	1.28	7.28E−2	1.23
5.00E−2	2.73E−2	2.27	1.96E−2	2.32	1.83E−2	2.64	1.10E−2	2.73
2.50E−2	5.13E−3	2.41	3.54E−3	2.47	3.44E−3	2.41	2.01E−3	2.45
1.25E−2	1.01E−3	2.35	6.50E−4	2.45	7.91E−4	2.12	4.69E−4	2.10
1.00E−2	6.36E−4	2.06	3.92E−4	2.26	5.40E−4	1.71	3.09E−4	1.86
6.25E−3	2.38E−4	2.09	1.40E−4	2.19	2.17E−4	1.93	1.23E−4	1.96

Table 3.3
Rotating transport with smooth solution, $\mathbb{P}_2$ approximation.

h	$\mathbb{P}_2$ Ent.				$\mathbb{P}_2$ Gal.			
	L^1	Rate	L^2	Rate	L^1	Rate	L^2	Rate
2.00E−1	7.08E−2	–	4.14E−2	–	9.01E−2	–	4.89E−2	–
1.00E−1	2.11E−2	1.75	1.24E−2	1.73	2.93E−2	1.62	1.64E−2	1.57
5.00E−2	4.63E−3	2.18	2.51E−3	2.31	5.61E−3	2.38	3.01E−3	2.45
2.50E−2	1.14E−3	2.02	6.04E−4	2.06	1.24E−3	2.17	6.60E−4	2.19
1.25E−2	3.10E−4	1.88	1.67E−4	1.86	3.29E−4	1.93	1.77E−4	1.90
1.00E−2	1.95E−4	2.07	1.05E−4	2.08	2.04E−4	2.12	1.10E−4	2.13
6.25E−3	7.78E−5	1.96	4.20E−5	1.95	8.01E−5	1.99	4.32E−5	1.98

Table 3.4
Rotating transport with non-smooth solution, $\mathbb{P}_1$ approximation.

h	$\mathbb{P}_1$ Ent.				$\mathbb{P}_1$ Gal.			
	L^1	Rate	L^2	Rate	L^1	Rate	L^2	Rate
2.00E−1	7.00E−2	–	1.36E−1	–	7.72E−2	–	1.25E−1	–
1.00E−1	5.15E−2	0.44	1.14E−1	0.26	8.49E−2	–	1.33E−1	–
5.00E−2	2.78E−2	0.89	8.16E−2	0.48	5.53E−2	0.62	8.86E−2	0.59
2.50E−2	1.63E−2	0.77	6.13E−2	0.41	3.89E−2	0.51	6.69E−2	0.40
1.25E−2	9.77E−3	0.74	4.69E−2	0.39	2.78E−2	0.49	5.10E−2	0.39
1.00E−2	8.24E−3	0.77	4.30E−2	0.38	2.46E−2	0.54	4.65E−2	0.41
6.25E−3	5.83E−3	0.74	3.60E−2	0.37	1.94E−2	0.50	3.88E−2	0.39

solution is at most as accurate as the Galerkin approximation when the exact solution is smooth. We observe in Table 3.3 that indeed the $\mathbb{P}_2$ Galerkin approximation is second-order. This phenomenon is well-known to be induced by grid non-uniformity; third-order can be restored by using uniform grids.

We now focus our attention on a non-smooth solution. We consider a problem corresponding to the initial data $u_0(x,y) = \chi_{B(0,a)}(\sqrt{(x-r_0)^2+y^2})$ with parameters $a = 0.3$, $r_0 = 0.4$, where $\chi_{B(0,a)}$ denotes the characteristic function of the ball of radius a centered at the origin. The solution is in $L^\infty((0,t);\mathrm{BV}(\Omega))$. The theoretical convergence rates with respect to h in L^1 and L^2 are 1 and $\frac{1}{2}$, respectively. The results reported in Table 3.4 and Table 3.5 show that like in one space dimension the entropy viscosity solution is superior to the Galerkin solution, at least in the L^1-norm. We have also done tests with higher-order triangular finite elements up to $k = 12$ using the Fekete point strategy of [26], and we have observed that the convergence rates converge to the theoretical limits (1 and $\frac{1}{2}$, respectively) as the polynomial order increases.

3.2.2. Spectral element approximation

The two-dimensional transport problem (3.8) is now investigated using the spectral element method in the square $\Omega = (-1,1)^2$. The mesh is uniform and composed of identical square elements. The integration in time is done using the explicit RK4 scheme. The control parameters of the entropy viscosity are $c_E = 2$ and $c_{\max} = 0.05/k$ where we recall that k is the degree of the polynomial approximation.

The accuracy with respect to space is evaluated by considering the smooth solution to (3.8) generated by the initial condition $u_0(x,y) = \frac{1}{2}\left(1 - \tanh\left(\frac{(x-r_0)^2+y^2}{a^2} - 1\right)\right)$, with parameters $a = 0.3$, $r_0 = 0.4$. The errors are measured at time $t = 1$. We observe that the Galerkin method and the entropy viscosity method converge similarly with respect to the mesh size h and with respect to polynomial degree k. The L^1-norm of the error on the Galerkin solution is shown in the left panel of Fig. 3.3 as a function of the mesh size h for various polynomial degrees k. The L^1-norm of the error on the entropy solution

Please cite this article in press as: J.-L. Guermond et al., Entropy viscosity method for nonlinear conservation laws, J. Comput. Phys. (2011), doi:10.1016/j.jcp.2010.11.043

is shown in the right panel of Fig. 3.3 as a function of the polynomial degree k for various mesh-sizes. The test confirms again that the entropy viscosity vanishes for smooth solutions and thus preserves spectral accuracy.

We now test the behavior of the method on the non-smooth solution generated by the initial data $u_0(x,y) = \chi_{B(0,a)}(\sqrt{(x-r_0)^2+y^2})$ with parameters $a = 0.3$, $r_0 = 0.4$, where $\chi_{B(0,a)}$ denotes the characteristic function of the ball of radius a centered at the origin. The errors are measured at time $t = 1$. We show in Fig. 3.4 the L^1-norm of the error for both the Galerkin solution (left panel) and the entropy viscosity solution (right panel) as a function of the mesh-size for various polynomial degrees. The convergence rate of the Galerkin solution is approximately $\frac{1}{2}$ whereas it is close to optimality, i.e., 1, for the entropy viscosity solution.

Table 3.5
Rotating transport with non-smooth solution, $\mathbb{P}_2$ approximation.

h	$\mathbb{P}_2$ Ent.				$\mathbb{P}_2$ Gal.			
	L^1	Rate	L^2	Rate	L^1	Rate	L^2	Rate
2.00E−1	4.34E−2	–	1.09E−1	–	7.65E−2	–	1.27E−1	–
1.00E−1	2.38E−2	0.87	7.32E−2	0.58	5.02E−2	0.61	7.78E−2	0.71
5.00E−2	1.37E−2	0.80	5.57E−2	0.39	3.46E−2	0.54	5.80E−2	0.42
2.50E−2	8.04E−3	0.77	4.25E−2	0.39	2.54E−2	0.44	4.59E−2	0.34
1.25E−2	4.67E−3	0.78	3.24E−2	0.39	1.89E−2	0.43	3.69E−2	0.31
1.00E−2	3.94E−3	0.76	2.98E−2	0.37	1.72E−2	0.43	3.41E−2	0.35
6.25E−3	2.72E−3	0.79	2.48E−2	0.39	1.44E−2	0.38	2.90E−2	0.35

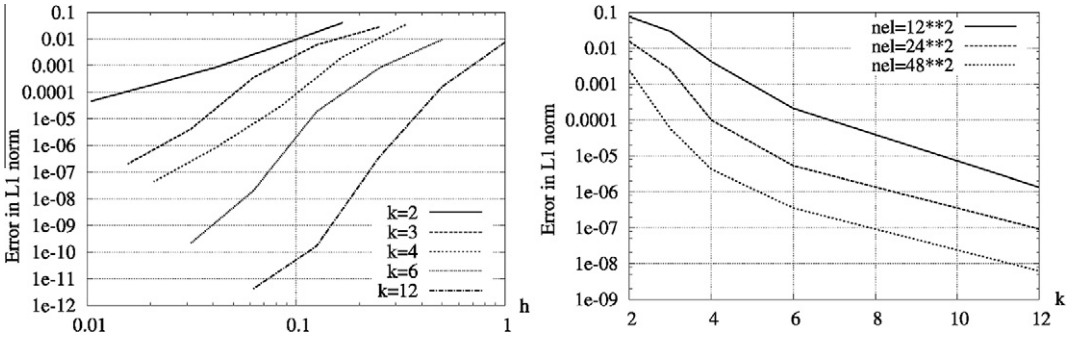

Fig. 3.3. Convergence tests with spectral element approximation on smooth solution. Left: Galerkin solution; L^1-norm of error versus mesh size h for various polynomial degrees k. Right: Entropy viscosity solution; L^1-norm of error versus k for various mesh-sizes h.

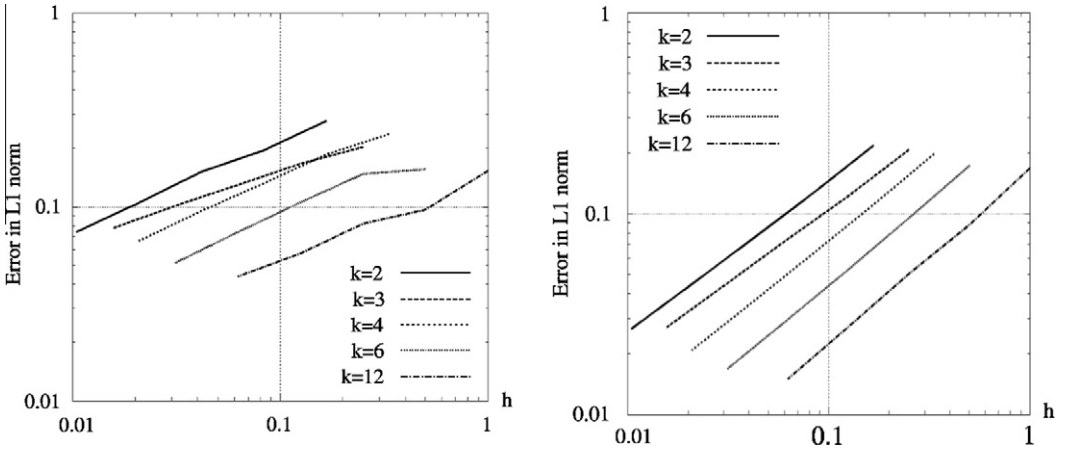

Fig. 3.4. Convergence tests with the spectral element approximation on the non-smooth solution. L^1-norm of the error vs. h for various k. Left: Galerkin. Right: Entropy viscosity.

Please cite this article in press as: J.-L. Guermond et al., Entropy viscosity method for nonlinear conservation laws, J. Comput. Phys. (2011), doi:10.1016/j.jcp.2010.11.043

4. Non-linear conservation laws

The purpose of this section is to evaluate the accuracy of the entropy viscosity method when solving non-linear scalar conservation equations.

4.1. Inviscid burgers equation

We consider the inviscid Burgers equation in two space dimensions

$$\partial_t u + \nabla \cdot \left(\frac{1}{2}u^2 \boldsymbol{v}\right) = 0, \tag{4.1}$$

where $\boldsymbol{v} = (1,1)$ is a constant vector field, subject to the following initial condition

$$u(x,y,0) = u_0(x,y) = \begin{cases} -0.2 & \text{if } x < 0.5 \quad \text{and} \quad y > 0.5, \\ -1 & \text{if } x > 0.5 \quad \text{and} \quad y > 0.5, \\ 0.5 & \text{if } x < 0.5 \quad \text{and} \quad y < 0.5, \\ 0.8 & \text{if } x > 0.5 \quad \text{and} \quad y < 0.5. \end{cases} \tag{4.2}$$

The exact solution to this problem for $t > 0$ is as follows:

$$u(x,y,t) = \begin{cases} -0.2 \\ 0.5 \end{cases} \text{if } x < \tfrac{1}{2} - \tfrac{3t}{5} \quad \text{and} \quad \begin{cases} y > \tfrac{1}{2} + \tfrac{3t}{20}, \\ \text{otherwise}, \end{cases}$$
$$\begin{cases} -1 \\ 0.5 \end{cases} \text{if } \tfrac{1}{2} - \tfrac{3t}{5} < x < \tfrac{1}{2} - \tfrac{t}{4} \quad \text{and} \quad \begin{cases} y > -\tfrac{8x}{7} + \tfrac{15}{14} - \tfrac{15t}{28}, \\ \text{otherwise}, \end{cases}$$
$$\begin{cases} -1 \\ 0.5 \end{cases} \text{if } \tfrac{1}{2} - \tfrac{t}{4} < x < \tfrac{1}{2} + \tfrac{t}{2} \quad \text{and} \quad \begin{cases} y > \tfrac{x}{6} + \tfrac{5}{12} - \tfrac{5t}{24}, \\ \text{otherwise}, \end{cases} \tag{4.3}$$
$$\begin{cases} -1 \\ \frac{2x-1}{2t} \end{cases} \text{if } \tfrac{1}{2} + \tfrac{t}{2} < x < \tfrac{1}{2} + \tfrac{4t}{5} \quad \text{and} \quad \begin{cases} y > x - \tfrac{5}{18t}\left(x + t - \tfrac{1}{2}\right)^2, \\ \text{otherwise}, \end{cases}$$
$$\begin{cases} -1 \\ 0.8 \end{cases} \text{if } x > \tfrac{1}{2} + \tfrac{4t}{5} \quad \text{and} \quad \begin{cases} y > \tfrac{1}{2} - \tfrac{t}{10}, \\ \text{otherwise}. \end{cases}$$

The entropy pair that we choose for this problem is $\left(E(u) = \frac{1}{2}u^2, \boldsymbol{F}(u) = \frac{1}{3}u^3\boldsymbol{v}\right)$. The solution is computed at $t = 0.5$ to facilitate comparisons with [5,14].

4.1.1. Inviscid Burgers/finite elements

The entropy viscosity solution is computed in $\Omega = (0,1)^2$ with $\mathbb{P}_1$ and $\mathbb{P}_2$ finite elements using $c_{\max} = 0.4/k$ and $c_E = 1$. The initial data is shown in the left panel of Fig. 4.1. The $\mathbb{P}_1$ entropy viscosity solution computed on a mesh composed of $3\,10^4$ nodes is shown in the right panel of Fig. 4.1. The shocks are very well captured.

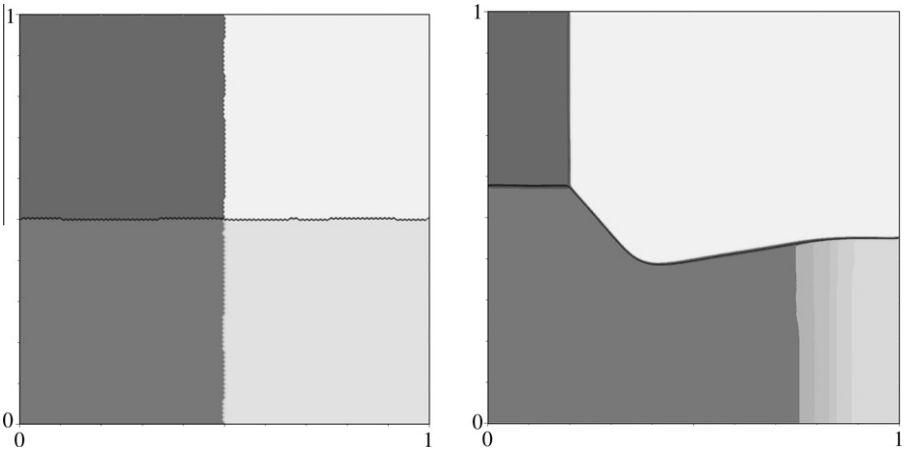

Fig. 4.1. Burgers test case. Left: Initial data. Right: $\mathbb{P}_1$ approximation at $t = 0.5$, $3\ 10^4$ nodes.

Please cite this article in press as: J.-L. Guermond et al., Entropy viscosity method for nonlinear conservation laws, J. Comput. Phys. (2011), doi:10.1016/j.jcp.2010.11.043

Errors and convergence rates are displayed in Table 4.1 for the $\mathbb{P}_1$ and $\mathbb{P}_2$ approximations. As expected, the convergence rates in the L^1- and L^2-norms are close to the optimal values 1 and $\frac{1}{2}$, respectively.

4.1.2. Inviscid Burgers/Fourier approximation

We now test the entropy viscosity method on the inviscid Burgers equation with Fourier expansions.

The computational domain is extended to $\widetilde{\Omega} = (0,2)^2$ and the initial data is extended by symmetry with respect to the axes $\{x = 1\}$ and $\{y = 1\}$ by setting

$$\tilde{u}_0(x,y) = \begin{cases} u_0(x,y) & \text{if } (x,y) \in (0,1)^2, \\ u_0(x,2-y) & \text{if } (x,y) \in (0,1)\times(1,2), \\ u_0(2-x,y) & \text{if } (x,y) \in (1,2)\times(0,1), \\ u_0(2-x,2-y) & \text{if } (x,y) \in (1,2)\times(1,2). \end{cases} \tag{4.4}$$

This extension makes the problem periodic.

The standard explicit RK4 scheme is used for the time approximation and the time-step is chosen such that the CFL number equals 0.2. The control parameters of the entropy viscosity are $c_{\max} = 0.5$ and $c_E = 8$. For every collocation point $\boldsymbol{x}$, the neighborhood $V_{\boldsymbol{x}}$ which is used to define the maximum local wave speed is composed of the 7×7 collocation points contained in the cube centered at $\boldsymbol{x}$ and of side $6h$. The smoothing operator S is realized by doubling the 5 grid-points average, so that 13 grid-points are eventually involved in the averaging. These local treatments do not have significant effects on the results, especially on the L^1- and L^2-norm of error. The effect is rather qualitative and noticeable only in the eye-ball norm.

The computations have been done with trigonometric polynomials of degree $N = \{36, 72, 144, 288\}$. When taking into account the de-aliasing $\frac{3}{2}$-rule and the extension of the domain, this gives 24^2, 48^2, 96^2 and 192^2 grid-points in the region $(0,1)^2$.

The numerical errors measured in the L^1- and L^2-norms together with the corresponding convergence rates are displayed in Table 4.2. As expected, the convergence rates are close to 1 and $\frac{1}{2}$ in the L^1- and L^2-norms, respectively. We have observed that these quantitative results are unchanged if no de-aliasing and no local averaging of the entropy viscosity is done.

The distribution of entropy viscosity computed at $t = 0.5$ for $N = 144$ and $N = 288$ is shown in Fig. 4.2 (96^2 and 192^2 grid-points in the region $(0,1)^2$, respectively). It is remarkable that the viscosity focuses very well in the shocks. Note that the slight smearing of the viscosity across the shocks is mainly due to the local averaging discussed before. Sharper and more focused viscosity fields can be obtained by removing the smoothing with no significant impact on the convergence rates.

4.2. KPP rotating wave/spectral elements

We now turn our attention to nonlinear scalar conservation equations with non-convex fluxes. We consider the following two-dimensional scalar conservation equation

$$\partial_t u + \nabla \cdot \boldsymbol{f}(u), \quad \boldsymbol{f}(u) = (\sin u, \cos u), \quad u(x,y,0) = \begin{cases} 3.5\pi, & x^2 + y^2 < 1, \\ 0.25\pi, & \text{otherwise.} \end{cases} \tag{4.5}$$

The local velocity is $\boldsymbol{f}'(u) = (\cos u, -\sin u)$. This test was proposed in [19] and is challenging to many high-order numerical schemes because the solution has a two-dimensional composite wave structure. For example central-upwind schemes based on WENO5, Minmod 2 and SuperBee reconstructions fail in this test case; see [19] for details.

Table 4.1
Convergence tests, inviscid Burgers equation. Left: $\mathbb{P}_1$ approximation. Right: $\mathbb{P}_2$ approximation.

h	$\mathbb{P}_1$				$\mathbb{P}_2$			
	L^2	Rate	L^1	Rate	L^2	Rate	L^1	Rate
5.00E−2	2.36E−1	–	9.37E−2	–	1.81E−1	–	5.25E−2	–
2.50E−2	1.76E−1	0.42	4.99E−2	0.91	1.30E−1	0.48	2.72E−2	0.95
1.25E−2	1.28E−1	0.46	2.60E−2	0.94	9.55E−2	0.44	1.46E−2	0.90
6.25E−3	9.36E−2	0.45	1.36E−2	0.94	6.88E−2	0.47	7.64E−3	0.93
3.12E−3	6.75E−2	0.47	6.98E−3	0.96	–	–	–	–

Table 4.2
Convergence tests, inviscid Burgers. Fourier approximation.

h	L^1	Rate	L^2	Rate
4.35E−2	1.92E−2	–	1.02E−1	–
2.13E−2	9.99E−3	0.94	7.28E−2	0.49
1.05E−3	5.34E−3	0.89	5.41E−2	0.43
5.24E−3	2.79E−3	0.95	3.80E−2	0.51

Please cite this article in press as: J.-L. Guermond et al., Entropy viscosity method for nonlinear conservation laws, J. Comput. Phys. (2011), doi:10.1016/j.jcp.2010.11.043

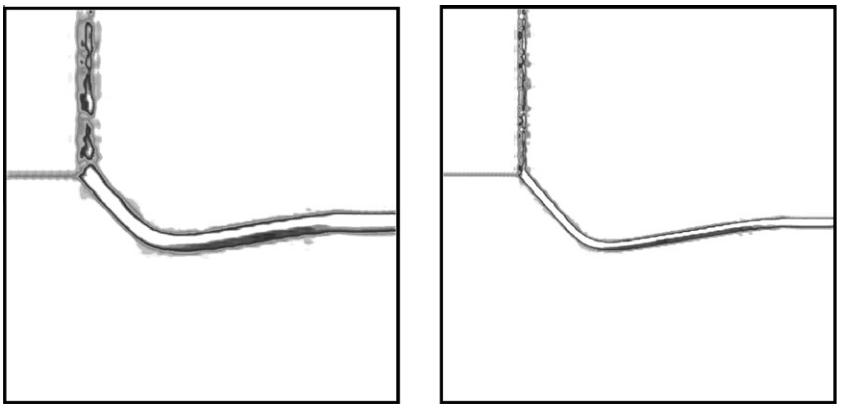

Fig. 4.2. Entropy viscosity for the 96×96 grid, $0 < v_h < 0.0050$ (at left), and for the 192×192 grid, $0 < v_h < 0.025$ (at right).

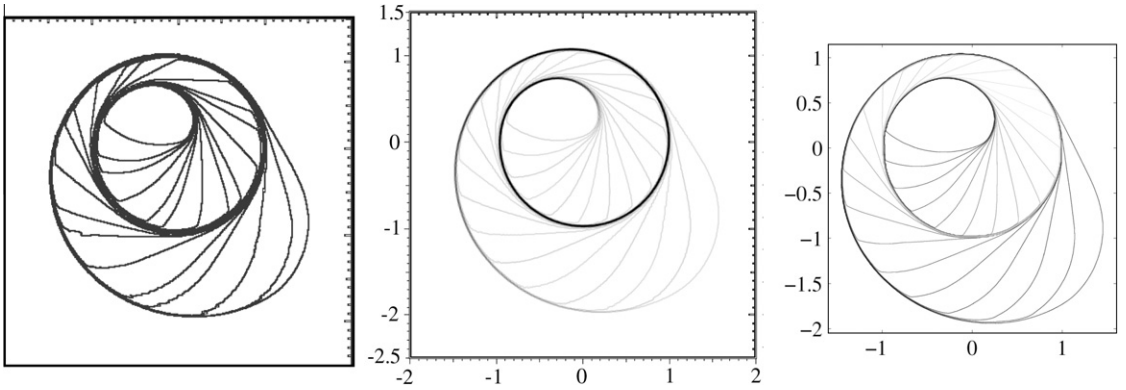

Fig. 4.3. KPP rotating wave. Left: Entropy–viscosity with spectral elements, $k = 4$ on 96^2 elements. Center: entropy–viscosity $\mathbb{P}_2$ approximation, $h = 0.0125$. Right: adaptive WENO5/Minmod 1 from [19] on Cartesian grid $\Delta x = \Delta y = \frac{1}{100}$.

The entropy viscosity solution is computed using spectral elements and the entropy pair: $E(u) = \frac{1}{2}u^2, \boldsymbol{F}(u) = (u \sin u + \cos u, u \cos u - \sin u)$. The control parameters of the entropy viscosity are $c_E = 40$ and $c_{\max} = 0.8/k$. The local smoothing of the viscosity is done through averaging over the closest five Gauss–Lobatto-Legendre points using the trapezoidal rule (2.18).

Iso-contours of the solution computed at $t = 1$ are shown in Fig. 4.3. The spectral element solution shown in the left panel has been computed using polynomials of degree $k = 4$ on a uniform mesh composed of 96^2 spectral elements. The solution shows the expected rotating composite wave structure. The spectral element solution is compared with the $\mathbb{P}_2$ entropy viscosity solution computed on a triangular mesh composed of 29857 $\mathbb{P}_2$ nodes (center panel), and an adaptive WENO5/Minmod 1 solution from [19] on a Cartesian grid $\Delta x = \Delta y = \frac{1}{100}$ (right panel).

The ratio $v_E/v_{\max}$ computed by the spectral element method on two grids, 48^2 and 96^2 elements with $k = 4$, is shown in Fig. 4.4. As expected, dissipation is added in the shock region only and the ratio $v_E/v_{\max}$ saturates to 1 in this region.

4.3. Buckley–Leverett equation with gravity/finite elements

We consider the Buckley–Leverett equation with gravitational effects in the y-direction

$$\partial_t u + \nabla \cdot \boldsymbol{f}(u) = 0 \quad u(x,y,0) = \begin{cases} 1.0, & x^2 + y^2 < 0.5; \\ 0.0, & \text{otherwise.} \end{cases}, \tag{4.6}$$

where $\boldsymbol{f}(u) = \left(\frac{u^2}{u^2+(1-u)^2}, \frac{u^2(1-5(1-u)^2)}{u^2+(1-u)^2}\right)$. This example is considered in [16,5]. Again, the main difficulty of this problem is that the flux is non convex and the solution contains a two-dimensional composite wave structure.

The entropy viscosity solution computed at $t = 0.5$ with $\mathbb{P}_2$ finite elements on a triangular mesh composed of 66957 $\mathbb{P}_2$ nodes is shown in the left panel of Fig. 4.5. The time marching is done with the SSP RK3 method, see [10]. (The results do not depend on the time marching technique though.) The control parameters of the entropy viscosity are $c_{\max} = 0.5/k$ and

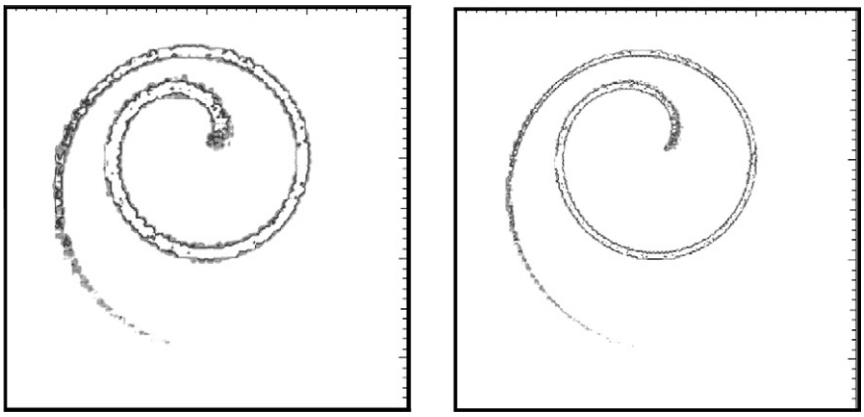

Fig. 4.4. KPP rotating wave. Ratio $v/v_{\max}$ for 48^2 and 96^2 elements. In both case the ratio saturates at $v/v_{\max} = 1$, with $v_{\max} \approx 0.016$ and $v_{\max} \approx 0.008$, respectively.

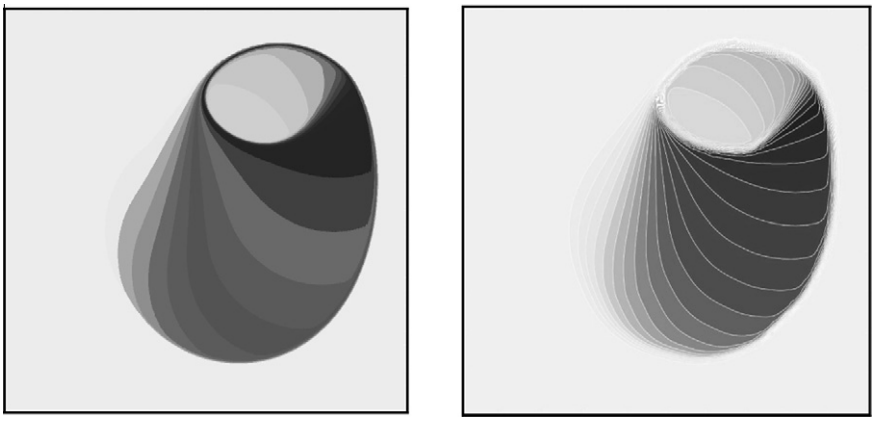

Fig. 4.5. Buckley-Leverett test case. Left: $\mathbb{P}_2$ approximation, $t = 0.5$, 6.710^4 nodes; Right $\mathbb{P}_1$ results using MAPR from [5] on uniform mesh with 10^4 nodes.

$c_E = 2$. The right panel shows the solution obtained in [5] with a $\mathbb{P}_1$ finite volume technique and a novel two-dimensional limiter methodology. The composite wave of the entropy viscosity solution is well captured and the shock region is sharper than the one from [5].

5. Euler equations of gas dynamics

We extend in this section the entropy viscosity method to the gas dynamics of perfect gases.

5.1. The Euler equations

We consider the Euler equations for a perfect gas in conservative form (see, e.g., [21]):

$$\partial_t \boldsymbol{c} + \nabla \cdot (\boldsymbol{f}(\boldsymbol{c})) = 0, \quad \boldsymbol{c} = \begin{pmatrix} \rho \\ \boldsymbol{m} \\ E \end{pmatrix}, \quad \boldsymbol{f}(\boldsymbol{c}) = \begin{pmatrix} \boldsymbol{m} \\ \boldsymbol{m} \otimes \frac{\boldsymbol{m}}{\rho} + p\mathbb{I} \\ \frac{\boldsymbol{m}}{\rho}(E+p) \end{pmatrix}, \tag{5.1}$$

where the independent variables are the density ρ, the momentum vector field $\boldsymbol{m}$ and the total energy E. The velocity vector field $\boldsymbol{u}$ is defined by $\boldsymbol{u} := \boldsymbol{m}/\rho$. The symbol $\mathbb{I}$ denotes the identity matrix in $\mathbb{R}^d$. The pressure is expressed via the equation of state of ideal gases:

$$p = \rho T, \quad \text{with} \quad T = (\gamma - 1)\left(\frac{E}{\rho} - \frac{1}{2}\boldsymbol{u}^2\right), \tag{5.2}$$

where γ is the adiabatic constant and T is the temperature. The Euler system is known to have a physical entropy functional

$$S(p, \rho) = \frac{\rho}{\gamma - 1} \log(p/\rho^\gamma). \tag{5.3}$$

Please cite this article in press as: J.-L. Guermond et al., Entropy viscosity method for nonlinear conservation laws, J. Comput. Phys. (2011), doi:10.1016/j.jcp.2010.11.043

This quantity satisfies the following inequality

$$\partial_t S + \nabla \cdot (\boldsymbol{u} S) \geqslant 0 \tag{5.4}$$

with equality if all the fields are smooth.

5.2. Fourier approximation

We specialize the algorithm to the Fourier approximation in this section.

5.2.1. Definition of the control parameters

Following [12], we replace the Euler system by the Navier–Stokes system where the viscosity and the thermal diffusivity are proportional to the entropy residual. Setting $\nabla^s \boldsymbol{u}_h := \frac{1}{2}(\nabla \boldsymbol{u}_h + (\nabla \boldsymbol{u}_h)^T)$, the additional viscous fluxes to consider are as follows:

$$\boldsymbol{f}_{visc}(\boldsymbol{c}_h) = \begin{pmatrix} 0 \\ -\mu_h \nabla^s \boldsymbol{u}_h \\ -\mu_h \nabla^s \boldsymbol{u}_h \cdot \boldsymbol{u}_h - \kappa_h \nabla T_h \end{pmatrix}. \tag{5.5}$$

Note that the Navier–Stokes viscous fluxes are compatible with the entropy inequality (5.4). One could also think of introducing viscous fluxes that dissipate the conservative variables, but these fluxes would be incompatible with (5.4).

The first step of the evaluation of the entropy viscosity consists of computing the residual of the entropy equation at every collocation point:

$$D_h(\boldsymbol{x}_{\boldsymbol{l}}, t) = \partial_t S_h(\boldsymbol{x}_{\boldsymbol{l}}, t) + \nabla \cdot (\boldsymbol{u}_h(\boldsymbol{x}_{\boldsymbol{l}}, t) S_h(\boldsymbol{x}_{\boldsymbol{l}}, t)), \quad \forall \boldsymbol{x}_{\boldsymbol{l}},\ \forall t > 0 \tag{5.6}$$

where the collocation points are defined in Section 2.5. Then we set

$$h(\boldsymbol{x}_{\boldsymbol{l}}) := h, \quad \forall \boldsymbol{x}_l, \tag{5.7}$$

$$R(D_h(\boldsymbol{x}_{\boldsymbol{l}}, t)) := |D_h(\boldsymbol{x}_{\boldsymbol{l}}, t)|, \quad \forall \boldsymbol{x}_{\boldsymbol{l}},\ \forall t > 0 \tag{5.8}$$

$$\mu_E(\boldsymbol{x}_{\boldsymbol{l}}, t) := c_E \rho_h(\boldsymbol{x}_{\boldsymbol{l}}, t) h^2(\boldsymbol{x}_{\boldsymbol{l}}) |D_h(\boldsymbol{x}_{\boldsymbol{l}}, t)|, \quad \forall \boldsymbol{x}_{\boldsymbol{l}},\ \forall t > 0. \tag{5.9}$$

The quantity μ_E is a dynamic viscosity.

To evaluate the maximum dynamic viscosity we set $h_{\max}(\boldsymbol{x}) = h$ and denote by $V_{\boldsymbol{x}}$ the set of $(2s+1)^d$ collocation points contained in the cube centered at $\boldsymbol{x}$ and of side $2sh$, (in practice we take $s = 3$). Using the upper bound on the local wave speed $|\boldsymbol{u}_h| + \sqrt{\gamma T_h}$, we set

$$\mu_{\max}(\boldsymbol{x}_{\boldsymbol{l}}, t) = c_{\max} h \max_{\boldsymbol{x}_{\boldsymbol{l}} \in V_{\boldsymbol{x}}} (|u_h(\boldsymbol{x}_{\boldsymbol{l}}, t)| + \sqrt{\gamma T_h(\boldsymbol{x}_{\boldsymbol{l}}, t)}). \tag{5.10}$$

Finally we set

$$\mu_h = S(\min(\mu_{\max}, \mu_E)), \quad \kappa_h = \frac{\mathcal{P}}{\gamma - 1} \mu_h, \tag{5.11}$$

where S is the multidimensional extension of the trapezoidal quadrature rule, typically involving 5 points in two space dimensions and 7 points in three space dimensions, see (2.18). The quantity $\mathcal{P} \approx 1$ is an artificial Prandtl number.

Remark 5.1. We have slightly simplified the strategy developed in [12] to evaluate μ_h and κ_h: the viscous and thermal stabilization terms are not included in the entropy residual. (Note that the same simplification has already been made in Section 4.1.2.)

5.2.2. Riemann problem; Case # 12

The method is now tested by considering a classical benchmark problem (benchmark # 12 from [23]). It is a two-dimensional Riemann problem developing complex structures involving shocks and contacts. The heat capacity ratio is $\gamma = 1.4$ and the initial data in $\Omega = (0,1)^2$ is defined to be

$$\begin{aligned} &p = 1, \quad \rho = 4/5, \quad \boldsymbol{u} = (0,0) \quad 0 < x < 1/2, \quad 0 < y < 1/2, \\ &p = 1, \quad \rho = 1, \quad \boldsymbol{u} = (3/\sqrt{17}, 0) \quad 0 < x < 1/2, \quad 1/2 < y < 1, \\ &p = 1, \quad \rho = 1, \quad \boldsymbol{u} = (0., 3/\sqrt{17}), \quad 1/2 < x < 1, \quad 0 < y < 1/2, \\ &p = 2/5, \quad \rho = 17/32, \quad \boldsymbol{u} = (0,0), \quad 1/2 < x < 1, \quad 0.5 < y < 1. \end{aligned} \tag{5.12}$$

We periodize the problem by extending the domain to $\widetilde{\Omega} = (0,2)^2$ and by extending the initial data by reflection about the axes $\{x = 1\}$, $\{y = 1\}$. Due to the finite speed of propagation of perturbations in this problem, the restriction to $(0,1)^2$ of the

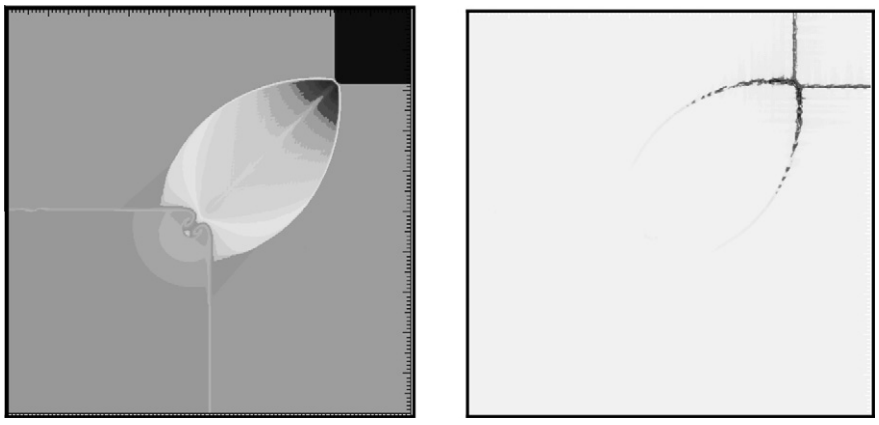

Fig. 5.1. Riemann problem # 12, $t = 0.2$, 400×400 grid-points. Left: Density, $0.528 \leqslant \rho_h \leqslant 1.707$. Right: Viscosity, $0 \leqslant \mu_h < 3.410^{-3}$.

solution to the periodized problem is identical to the restriction to $(0,1)^2$ of the solution to the Riemann problem in $\mathbb{R}^2$ up to time $t^* := \frac{s}{2(s^2+0.6)} > 0.32$, where $s = \frac{3}{\sqrt{17}}$.

The control parameters of the entropy viscosity are $c_{\max} = 0.5$, $c_E = 20$ and $\mathcal{P} = 1$. The time-step is defined so that the resulting CFL number is 1/3. For each collocation point $\boldsymbol{x}$, the local neighborhood, $V_{\boldsymbol{x}}$, which is used to define the maximum local wave speed at $\boldsymbol{x}$ is composed of the 7×7 collocation points closest to $\boldsymbol{x}$. The smoothing of the viscosity is done by a double sweep of the 5 points average defined in (2.18).

We show in the left panel of Fig. 5.1 the density field at $t = 0.2 < t^*$ on a 400×400 grid in $\Omega = (0,1)^2$. Taking into account the extension of the domain and the $\frac{3}{2}$-de-aliasing rule we used a 1201×1201 grid in $\widetilde{\Omega} = (0,2)^2$, i.e., we used $N = 600$. The Fourier result compares well with those from [23]. The shocks and the fine structures that develop behind them are very well described. The viscosity field is shown in the right panel of the figure. It is clear that the viscosity focuses well in the shocks; in particular, there is almost no viscosity along the two contact discontinuities.

5.3. Finite element approximation

We specialize the finite element setting to the Euler equations in this section. All the numerical tests reported in this section have been done by using the explicit SSP RK3 time integration.

5.3.1. Definition of the control parameters

Let the finite element approximation space X_h be defined as in Section 2.3. All the scalar-valued independent variables and the Cartesian components of the momentum and velocity vector fields are approximated in X_h. Whenever required, Dirichlet boundary conditions are enforced strongly, i.e., the Dirichlet conditions are enforced in the finite element spaces.

Similarly to the Fourier approximation, the algorithm consists of introducing an artificial viscosity and an artificial thermal diffusivity in the spirit of the Navier–Stokes equations. But at variance with the Fourier technique some stabilization is sometimes needed in the mass conservation equation for reason not yet fully understood, see Remark 5.2. The viscous flux vector is defined to be as follows

$$\boldsymbol{f}_{visc}(\boldsymbol{c}_h) = \begin{pmatrix} -\nu_h \nabla \rho_h \\ -\mu_h \nabla^s \boldsymbol{u}_h \\ -\mu_h \nabla^s \boldsymbol{u}_h \cdot \boldsymbol{u}_h - \kappa_h \nabla T_h \end{pmatrix}. \tag{5.13}$$

Note that these viscous fluxes are also compatible with the entropy inequality (5.4). The additional mass diffusion is compatible with the mass conservation since $-\operatorname{sgn}(\rho_h)\nabla\cdot(\nu_h \nabla \rho_h)$ formally converges to a positive measure as $h \to 0$, and it is also compatible with (5.4) since it formally yields

$$\partial_t S_h + \nabla \cdot (\boldsymbol{u}_h S_h - \kappa_h \nabla(\log(T_h)) + \nu_h \nabla \rho_h) \geqslant \frac{\mu_h}{T_h} \nabla^s \boldsymbol{u}_h : \nabla^s \boldsymbol{u}_h + \frac{\kappa_h}{T_h^2} \nabla T_h \cdot \nabla T_h. \tag{5.14}$$

The algorithm proceeds similarly to what is described in Section 2.2 and 2.3. At each time step we evaluate the residuals of the entropy equation and compute the associated artificial viscosities, then we update the mass, momentum, and total energy.

Please cite this article in press as: J.-L. Guermond et al., Entropy viscosity method for nonlinear conservation laws, J. Comput. Phys. (2011), doi:10.1016/j.jcp.2010.11.043

More specifically, for each mesh cell K in $\mathcal{T}_h$ the dynamic viscosity is computed as follows:

$$D_{h,1} := \partial_t S_h + \nabla \cdot (\boldsymbol{u}_h S_h), \tag{5.15}$$

$$D_{h,2} := \rho_h^{-1} S_h (\partial_t \rho_h + \nabla \cdot (\boldsymbol{u}_h \rho_h)), \tag{5.16}$$

$$\mu_E|_K := c_E \|\rho_h\|_{\infty,K} h_K^2 \max(\|D_{h,1}\|_{\infty,K}, \|D_{h,2}\|_{\infty,K}). \tag{5.17}$$

The second residual $D_{h,2}$ is meant to account for inaccuracies in mass conservation. Note that controlling $D_{h,2}$ and $D_{h,1}$ amounts to controlling the residual of the specific entropy, $s_h := \rho_h^{-1} S_h$, since

$$|\rho_h(\partial_t s_h + \boldsymbol{u}_h \cdot \nabla s_h)| = |D_{h,1} - D_{h,2}| \leqslant |D_{h,1}| + |D_{h,2}|.$$

The maximum dynamic viscosity, $\mu_{\max}$, is evaluated as follows:

$$\mu_{\max}|_K = c_{\max} h_K \|\rho_h\|_{\infty,K} \| |\boldsymbol{u}_h| + \sqrt{\gamma T_h} \|_{\infty,K}. \tag{5.18}$$

Finally we set:

$$\mu_h = \min(\mu_{\max}, \mu_E), \quad \kappa_h = \frac{\mathcal{P}}{\gamma - 1} \mu_h, \quad \nu_h = \frac{\mathcal{P}_\rho}{\|\rho_h\|_{\infty,K}} \mu_h, \tag{5.19}$$

where $\mathcal{P} = \mathcal{O}(1)$ and $\mathcal{P}_\rho = \mathcal{O}(1)$. Our experience is that using $\mathcal{P} \in [0, \frac{1}{4}]$ and $\mathcal{P}_\rho = [0, \frac{1}{10}]$ works well in most cases.

Remark 5.2. In all the numerical tests considered so far by the authors the algorithm was always observed to be stable with $\mathcal{P}_\rho = 0$ (i.e., without mass stabilization) provided the CFL was small enough. It happens sometimes that it is possible to increase the CFL up to 0.5 or above by using $\mathcal{P}_\rho \neq 0$. For instance in the Mach 3 Step test case (see Section 5.3.2) the algorithm is stable with $\mathcal{P} \geqslant 0.25, \mathcal{P}_\rho = 0$, and $CFL \leqslant 0.13$, but it is possible to make it stable up to CFL $\leqslant 0.5$ for $\mathcal{P} = 0.1$ by setting $\mathcal{P}_\rho = 0.1$. In some other cases, using $\mathcal{P}_\rho \neq 0$ can suppress residual oscillations on the density; hence, setting $\mathcal{P}_\rho \neq 0$ can be viewed as a filtering/cleaning mechanism.

5.3.2. Mach 3 step

We illustrate the algorithm described above by considering the Mach 3 flow in a wind tunnel with a forward facing step. The geometry of the domain is shown in Fig. 5.2. The initial data and inflow boundary conditions are specified in terms of the primitive variables

$$\left.\begin{array}{l}(\rho, \boldsymbol{u}, p)^T(x, y, 0) \\ (\rho, \boldsymbol{u}, p)^T(0, y, t)\end{array}\right\} = (1.4, (3.0, 0.0), 1.0)^T. \tag{5.20}$$

The outflow boundary at $\{x = 3\}$ is free. The slip condition $\boldsymbol{u} \cdot \boldsymbol{n} = 0$ is specified on the solid wall of the tunnel, $\boldsymbol{n}$ being the unit outward normal on $\partial\Omega$. This benchmark test has been proposed in [9] and has been popularized by Woodward and Colella's extensive study [32].

We show in Fig. 5.2 the density field at $t = 4$ on two different meshes with $\mathbb{P}_1$ Lagrange finite elements. The results shown in the left panels have been obtained on a mesh composed of 4813 $\mathbb{P}_1$ nodes and the results shown in the right panels have been obtained on a mesh composed of 893468 $\mathbb{P}_1$ nodes. These computations have been done with $c_{\max} = 0.25$, $c_E = 1$, $\mathcal{P} = 0.1$ and $\mathcal{P}_\rho = 0.1$. The tests have been run with CFL = 0.5. Our solutions agree, at least in the eye-ball norm, with other reference solutions that can be found in the literature. The contact discontinuity emerging from the three-shock interaction point is present in both simulations and is captured quite accurately. A Kelvin–Helmholtz instability develops along the contact discontinuity on the refined mesh.

As reported in [32] we have observed that the way the velocity boundary condition is implemented in the vicinity of the corner of the step somewhat influences the quality of the solution. We do not enforce any boundary condition at the node at the corner of the step in the computation, enforcing the slip condition at this particular point implies $\boldsymbol{u} = 0$, which is too strong a constraint.

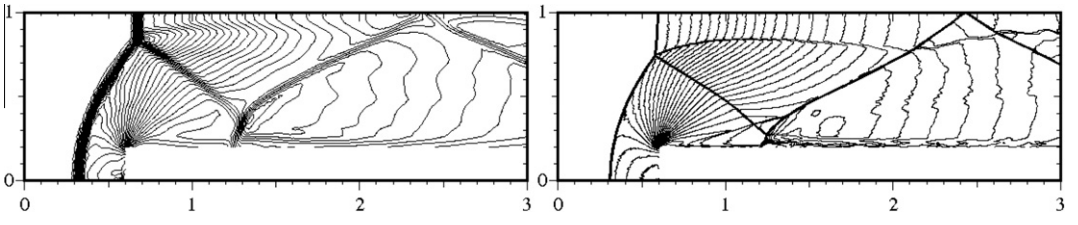

Fig. 5.2. Mach 3 step, density, $t = 4$, density, $\mathbb{P}_1$ approximation. Left: $h = 0.25, 4813\mathbb{P}_1$ nodes. Right: $h = 0.003, 893468\mathbb{P}_1$ nodes.

Please cite this article in press as: J.-L. Guermond et al., Entropy viscosity method for nonlinear conservation laws, J. Comput. Phys. (2011), doi:10.1016/j.jcp.2010.11.043

5.3.3. Double mach reflection

We now solve the so-called double Mach reflection problem at Mach 10. This problem, popularized by Woodward and Colella (see [32] for complete description), involves a Mach 10 shock in air ($\gamma = 1.4$) that impinges a wall with a 60° angle. The undisturbed air ahead of the shock has density 1.4 and pressure 1. The computational domain is $\Omega = (0,4) \times (0,1)$. The reflecting wall lies at the bottom of the domain and starts at $x = \frac{1}{6}$, i.e., free slip boundary condition is enforced on $\{x \geqslant \frac{1}{6}, y = 0\}$. The shock makes a 60° angle with the x-axis. Outflow boundary conditions are enforced at $\{0 \leqslant x < \frac{1}{6}, y = 0\}$ and $\{x = 4\}$. The boundary values along the top boundary $\{y = 1\}$) are set to describe the motion of the

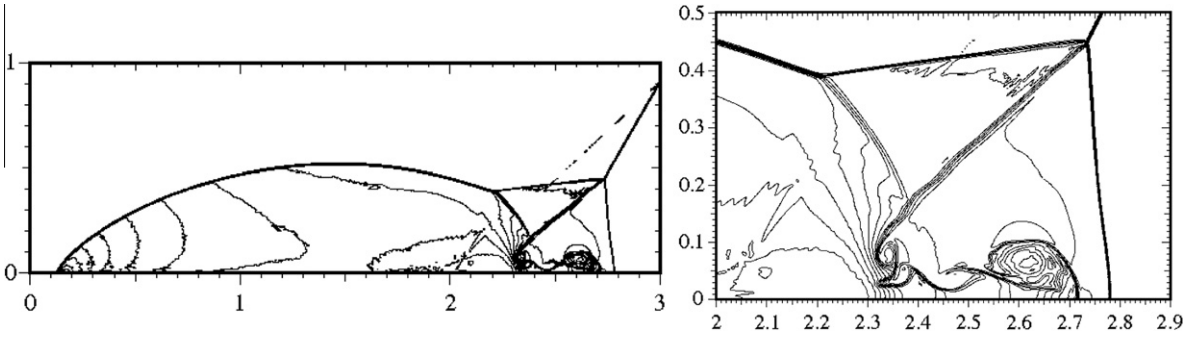

Fig. 5.3. Double Mach reflection at $t = 0.2$, $M = 10$, density field, 453969 $\mathbb{P}_1$ nodes. Left: global view. Right: close up view in the region of three-shock interaction point.

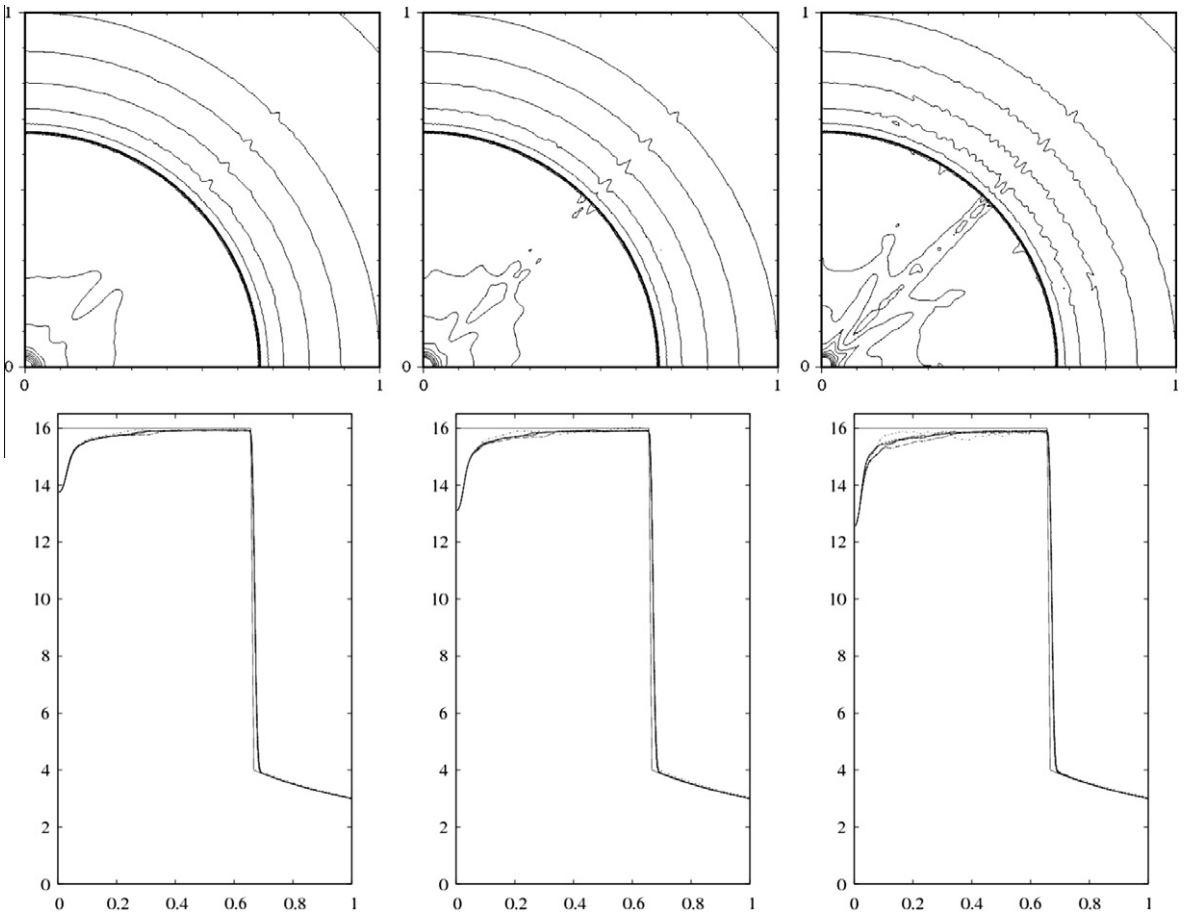

Fig. 5.4. Noh test case at time $t = 2$. Top: 23 density contours (from 2.5 to 4 with step 0.25 and from 14 to 17 with step 0.2). Bottom: Density profile versus radius along segments $(r \in (0,1), \theta \in \{0, \frac{\pi}{8}, \frac{\pi}{4}, \frac{3\pi}{8}, \frac{\pi}{2}\}$. Left panels: $\mathcal{P} = 1$. Center panel: $\mathcal{P} = \frac{1}{2}$. Right panel: $\mathcal{P} = \frac{1}{4}$.

Please cite this article in press as: J.-L. Guermond et al., Entropy viscosity method for nonlinear conservation laws, J. Comput. Phys. (2011), doi:10.1016/j.jcp.2010.11.043

initial Mach 10 shock. The flow is computed at time $t = 0.2$. The control parameters of the entropy viscosity are $c_{\max} = 0.25$, $c_E = 0.25$, $\mathcal{P} = 0.075$ and $\mathcal{P}_\rho = 0$. The tests have been run with CFL = 0.5.

We show in Fig. 5.3 the solution computed with $\mathbb{P}_1$ Lagrange polynomials on a mesh composed of 453969 nodes. The left panel displays the density field in the region $0 \leqslant x \leqslant 3$. The right panel shows a close up view of the density in the region of the three-shock interaction point. The location of the head of the jet coincide with the value usually reported in the literature (between 2.71 and 2.74).

5.3.4. Noh problem

We finish this series of tests with the test of Noh [24] for an ideal gas with $\gamma = \frac{5}{3}$. This is a Cauchy problem in $\mathbb{R}^2$. The initial data is

$$(\rho, \boldsymbol{u}, p) = \left(1, -(x,y)(x^2+y^2)^{-\frac{1}{2}}, 0\right). \tag{5.21}$$

To avoid singularities when computing the entropy, we set the initial pressure to 10^{-6} as recommended in [23]. We observed that using 10^{-9} as the initial pressure does not change our results. The initial velocity field is circularly symmetric, directed toward the origin with magnitude 1. This problem has an exact solution. It is a circularly symmetric shock reflecting from the origin. The shock speed is $\frac{1}{3}$. Behind the shock, i.e., $\sqrt{x^2+y^2} < \frac{1}{3}t$ the density is 16, the velocity is 0, and the pressure is $\frac{16}{3}$. Ahead of the shock, i.e., for $\sqrt{x^2+y^2} > \frac{1}{3}t$, the density is $(1 + t/\sqrt{x^2+y^2})$, while velocity and pressure are equal to their respective initial value. The computational domain is $\Omega = (0,1)^2$. We use the exact density, pressure, and velocity at the boundaries $\{x = 1\}$ and $\{y = 1\}$. At the other two boundaries $\{x = 0\}$ and $\{y = 0\}$ nothing is enforced on ρ (natural boundary condition), but $\boldsymbol{u}\cdot\boldsymbol{n} = 0$ is enforced on the velocity. As reported in [23] most methods dealing with this problem suffer from a very large error in the density at the center.

We have solved this problem with $c_E = 0.25, \mathcal{P}_\rho = 0.025$ and made various tests with $\mathcal{P} \in \{\frac{1}{4}, \frac{1}{2}, 1\}$. The tests have been run with CFL = 0.5 with $\mathbb{P}_1$ finite elements on a mesh composed 59098 triangles and 29870 nodes, $h \approx 0.00625$. The density field at $t = 2$ is shown in Fig. 5.4. The top panels show the iso-values of the density from 2.5 to 4 with step 0.25 and from 14 to 17 with step 0.2 as done in [23]. The bottom panels show radial profiles of the density field versus radius along nine segments $(r \in (0,1), \theta \in \{0, \frac{\pi}{16}, \ldots, \frac{7\pi}{16}, \frac{\pi}{2}\}$. The results in the left panels have been obtained with $\mathcal{P} = 1$, those in the center with $\mathcal{P} = 0.5$, and those in the right with $\mathcal{P} = 0.25$. These results are comparable with those reported in [23]. It seems that density error at the center decreases as $\mathcal{P}$ increases.

The code runs with $\mathcal{P}_\rho = 0$, but the density field in the vacuum region develops small oscillations. Using $\mathcal{P}_\rho = 0.025$ can be viewed as a filtering mechanism for visualization purpose.

6. Conclusions

A new class of high-order numerical methods for approximating nonlinear conservation laws has been proposed (entropy viscosity method). It can be applied to any equation or system that admit one or more entropy inequalities and that can be regularized in ways that are compatible with these entropy inequalities. The principle of the method can be summarized as follows: assuming that a centered discretization of the conservation equations with a linear first-order viscosity is at hand and that the first-order viscosity is large enough to make the method monotone, then the entropy viscosity method consists of constructing a new viscosity proportional the local size of the entropy production and replacing the first-order viscosity by the minimum of the first-order viscosity and the entropy viscosity. The underlying heuristics is that in regions where the entropy production is large, the entropy viscosity is large as well and the effective viscosity is limited to be first-order, thus making the method monotone in these regions. In smooth regions the entropy production is small (of the same order as the truncation error of the centered approximation method) and the effective viscosity is negligible. This new approach is very simple to implement on unstructured grids since it does not use any flux or slope limiters. Of course, the method cannot be applied to conservation equations that are not known to have entropies.

Although the method seems to behave quite well on many benchmark problems, the amount of theory to justify the approach is almost non-existent. The justification of the method is mainly heuristic for the time being. The authors have recently proved stability of the method on the linear transport equation, but a lot more theoretical investigation still need to be done to fully understand the method.

References

[1] A. Bonito, J-L. Guermond, B. Popov, Convergence analysis of the entropy viscosity method, 2010, in preparation.
[2] J.G. Andrews, K.W. Morton, A posteriori error estimation based on discrepancies in an entropy variable, Int. J. Comput. Fluid Dyn. 10 (3) (1998) 183–198.
[3] C. Bardos, A.Y. le Roux, J.-C. Nédélec, First order quasilinear equations with boundary conditions, Commun. Partial Differ. Equat. 4 (9) (1979) 1017–1034.
[4] Erik Burman, Peter Hansbo, Edge stabilization for Galerkin approximations of convection–diffusion-reaction problems, Comput. Methods Appl. Mech. Eng. 193 (15–16) (2004) 1437–1453.
[5] Ivan Christov, Bojan Popov, New non-oscillatory central schemes on unstructured triangulations for hyperbolic systems of conservation laws, J. Comput. Phys. 227 (11) (2008) 5736–5757.
[6] Camillo De Lellis, Felix Otto, Michael Westdickenberg, Minimal entropy conditions for Burgers equation, Quart. Appl. Math. 62 (4) (2004) 687–700.

Please cite this article in press as: J.-L. Guermond et al., Entropy viscosity method for nonlinear conservation laws, J. Comput. Phys. (2011), doi:10.1016/j.jcp.2010.11.043

[7] M.O. Deville, P.F. Fischer, E.H. Mund, High-order methods for incompressible fluid flow, Cambridge Monographs on Applied and Computational Mathematics, vol. 9, Cambridge University Press, Cambridge, 2002.
[8] Jim Douglas Jr., Todd Dupont, Interior penalty procedures for elliptic and parabolic Galerkin methods, in: Computing Methods in Applied Sciences (Second International Symposium, Versailles, 1975), Lecture Notes in Physics, vol. 58, Springer, Berlin, 1976, pp. 207–216.
[9] Ashley F. Emery, An evaluation of several differencing methods for inviscid fluid flow problems, J. Comput. Phys. 2 (1968) 306–331.
[10] Sigal Gottlieb, Chi-Wang Shu, Eitan Tadmor, Strong stability-preserving high-order time discretization methods, SIAM Rev. 43 (1) (2001) 89–112. electronic.
[11] J.-L. Guermond, Stabilization of Galerkin approximations of transport equations by subgrid modeling, M2AN Math. Model. Numer. Anal. 33 (6) (1999) 1293–1316.
[12] J.-L. Guermond, R. Pasquetti, Entropy-based nonlinear viscosity for fourier approximations of conservation laws, C.R. Math. Acad. Sci. Paris 346 (2008) 801–806.
[13] T.J.R. Hughes, M. Mallet, A new finite element formulation for computational fluid dynamics. IV: A discontinuity-capturing operator for multidimensional advective–diffusive systems, Comput. Methods Appl. Mech. Eng. 58 (1986) 329–336.
[14] Guang-Shan Jiang, Eitan Tadmor, Nonoscillatory central schemes for multidimensional hyperbolic conservation laws, SIAM J. Sci. Comput. 19 (6) (1998) 1892–1917. electronic.
[15] C. Johnson, A. Szepessy, P. Hansbo, On the convergence of shock-capturing streamline diffusion finite element methods for hyperbolic conservation laws, Math. Comput. 54 (189) (1990) 107–129.
[16] K. Hvistendahl Karlsen, K. Brusdal, H.K. Dahle, S. Evje, K.-A. Lie, The corrected operator splitting approach applied to a nonlinear advection–diffusion problem, Comput. Methods Appl. Mech. Eng. 167 (3–4) (1998) 239–260.
[17] S.N. Kružkov, First order quasilinear equations with several independent variables, Mat. Sb. (N.S.) 81 (123) (1970) 228–255.
[18] Alexander Kurganov, Guergana Petrova, Central-upwind schemes on triangular grids for hyperbolic systems of conservation laws, Numer. Methods Partial Differ. Equat. 21 (3) (2005) 536–552.
[19] Alexander Kurganov, Guergana Petrova, Bojan Popov, Adaptive semidiscrete central-upwind schemes for nonconvex hyperbolic conservation laws, SIAM J. Sci. Comput. 29 (6) (2007) 2381–2401. electronic.
[20] Philippe G. LeFloch, Jian-Guo Liu, Generalized monotone schemes, discrete paths of extrema, and discrete entropy conditions, Math. Comput. 68 (227) (1999) 1025–1055.
[21] Randall J. LeVeque, Finite volume methods for hyperbolic problems, Cambridge Texts in Applied Mathematics, Cambridge University Press, Cambridge, 2002.
[22] P.-L. Lions, P.E. Souganidis, Convergence of MUSCL and filtered schemes for scalar conservation laws and Hamilton–Jacobi equations, Numer. Math. 69 (4) (1995) 441–470.
[23] Richard Liska, Burton Wendroff, Comparison of several difference schemes on 1D and 2D test problems for the Euler equations, SIAM J. Sci. Comput. 25 (3) (2003) 995–1017. electronic.
[24] W.F. Noh, Errors for calculations of strong shocks using an artificial viscosity and artificial heat flux, J. Comput. Phys. 72 (1) (1987) 78–120.
[25] E. Yu, Panov, Uniqueness of the solution of the Cauchy problem for a first-order quasilinear equation with an admissible strictly convex entropy, Mat. Zametki 55 (5) (1994) 116–129. 159.
[26] Richard Pasquetti, Francesca Rapetti, Spectral element methods on triangles and quadrilaterals: comparisons and applications, J. Comput. Phys. 198 (1) (2004) 349–362.
[27] Bojan Popov, Ognian Trifonov, One-sided stability and convergence of the Nessyahu–Tadmor scheme, Numer. Math. 104 (4) (2006) 539–559.
[28] Gabriella Puppo, Numerical entropy production for central schemes, SIAM J. Sci. Comput. 25 (4) (2003) 1382–1415.
[29] S. Rebay, Efficient unstructured mesh generation by means of Delaunay triangulation and Bowyer–Watson algorithm, J. Comput. Phys. 106 (1993) 125–138.
[30] C.W. Shu, S. Osher, Efficient implementation of essentially non-oscillatory shock-capturing schemes, II, J. Comput. Phys. 83 (1989) 32–78.
[31] A. Szepessy, Convergence of a shock-capturing streamline diffusion finite element method for a scalar conservation law in two space dimensions, Math. Comput. 53 (188) (1989) 527–545.
[32] Paul Woodward, Phillip Colella, The numerical simulation of two-dimensional fluid flow with strong shocks, J. Comput. Phys. 54 (1) (1984) 115–173.
[33] Huanan Yang, On wavewise entropy inequalities for high-resolution schemes. I. The semidiscrete case, Math. Comput. 65 (213) (1996) 45–67. S1–S13.
[34] Huanan Yang, On wavewise entropy inequality for high resolution schemes. II. Fully discrete MUSCL schemes with exact evolution in small time, SIAM J. Numer. Anal. 36 (1) (1999) 1–31. electronic.

Please cite this article in press as: J.-L. Guermond et al., Entropy viscosity method for nonlinear conservation laws, J. Comput. Phys. (2011), doi:10.1016/j.jcp.2010.11.043